Fuel 362 (2024) 130763

Contents lists available at ScienceDirect

Fuel

journal homepage: www.elsevier.com/locate/fuel

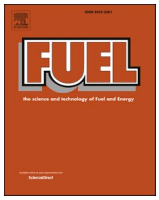

Full Length Article

Combustion performance and flame front morphology of producer gas from a biomass gasification-based cookstove

M. Reyes [a,*], J.F. Pérez [a,b], R. Sastre [a]

[a] Department of Energy and Fluid Mechanics Engineering, University of Valladolid, Paseo del Cauce s/n, E-47011 Valladolid, Spain
[b] Group of Efficient Management of Energy (GIMEL), Department of Mechanical Engineering, Faculty of Engineering, University of Antioquia, Calle 67 # 53-108, Medellín, Colombia

ARTICLE INFO

Keywords:
Biomass producer gas
Gasification
Cookstoves
Schlieren technique
Burning velocity
Combustion

ABSTRACT

The present work investigates the last phase of the biomass gasification-based cookstove, which is the combustion process of biomass producer gas (BGP). A constant volume combustion bomb and kinetic simulation are used to characterize the behavior of the biomass producer gas and its pollutant emissions under a conventional premixed combustion process. The BGP combustion processes of two types of biomasses available in Colombia (Pinus Patula and Cordia Alliodora) are studied under certain conditions of pressure, temperature, and equivalence ratio. To characterize the combustible mixture of gases obtained after biomass gasification, a combustion chamber with cylindrical geometry equipped with a Schlieren optical diagnostic system to visualize the combustion process, and a piezoelectric pressure transducer to register the instantaneous pressure are used. By visualizing the flame front, the flame propagation speed at which the flame propagates through the combustion chamber and the morphology of the flame are studied. Instantaneous pressure is the input of a two-zone diagnostic model through which variables, such as burning velocity, temperature, mass burned fraction, etc., are obtained to characterize the combustion process of the mentioned gasification gases. Experimental results are compared and complemented with kinetic modeling results obtained with the Cantera package using the GriMech 3.0 and Aramko 1.3 kinetic mechanisms, in terms of laminar burning velocity and NO, NO_2, CO, and CO_2 exhaust emissions. Results show that Cordia Alliodora presents higher burning velocities than Pinus Patula BP. However, lower CO_2 emissions are obtained during the Cordia Alliodora combustion, and NOx emissions are not influenced by the type of biomass considered.

1. Introduction

The access to clean technologies and fuels for cooking is crucial for reaching the sustainable development goals (SDG), aiming to improve health, reducing environmental impacts, and providing with alternatives of affordable and non-contaminating energy. Population at risk in remote areas is affected by the biomass use in traditional and inefficient systems (three stones cookfires) [1]. The use of biomass in traditional open-fire low-efficiency systems, which efficiency is about 10% [2], affects negatively the air indoor quality, causing health issues by the emission and exposition of people to pollutant emissions, such as carbon monoxide (CO) and particulate matter (PM) [3].

The 35% of the bioenergy used worldwide in 2021 were burned in traditional cookstoves (three stone fires); these assemblies with low efficiency led to increase polluting emissions, such as carbon monoxide and particulate matter, causing the death of 5 million people in 2021. The 2030 in the Net Zero Scenario drives the implementation of eco-efficient alternatives for the use of biomass, rather the traditional biomass uses, for contributing to the UN Sustainable Development Goal 7 on Affordable and Clean Energy. The 2030 carbon neutral scenario seeks to replace the traditional use of biomass in rural and isolated areas by cleaner energy sources such as biogas, bioethanol, and solid biomass in advanced cookstoves for more than 350 million of rural homes in 2030 [4].

In many countries there are programs of firewood biomass substitution for clean fuels such as natural gas, liquefied petroleum gas (LPG), and/or electricity. However, the difficult access to the most remote country's areas hinders the supply of clean fuels or energy for cooking; thus, the biomass will continue been the main energy source used as fuel in these remote regions. Therefore, the use of efficient stoves for firewood cooking demands advanced cookstove designs that use biomass as

* Corresponding author.
E-mail address: miriam.reyes@uva.es (M. Reyes).

https://doi.org/10.1016/j.fuel.2023.130763
Received 26 May 2023; Received in revised form 24 December 2023; Accepted 26 December 2023
Available online 10 January 2024

Nomenclature

Latin symbols

T	Temperature [K]
R	Radius [m] or [cm]
A	Area [m^2] or [cm^2]
m	Mass [kg] or [g]
Sn	Flame propagation speed [m/s]
un	Stretched burning velocity [m/s]
ul	Unstretched burning velocity [m/s]
u	Burning velocity [m/s]
L	Markstein length [m]
p	Pressure [MPa]
X	Mole fraction

Greek symbols

ρ	Density [kg/m^3]
α	Strain rate contribution to the stretch [s^{-1}]
α	Temperature exponent [dimensionless]
β	Pressure exponent [dimensionless]

Subscript symbols

i	Initial condition
f or flame	Referred to the flame
l	Referred to a unstretched laminar flame
b	Referred to the gas burned
ub	Referred to the unburned gas
n	Referred to a stretched laminar flame
0	Reference conditions

Superscript symbols

P	Obtained by pressured register

Symbols with special characters

wt %	Percentage of weight content [%]
vol%	Percentage of volume content [%]
κ	Stretch rate [s^{-1}]

Acronyms

BPG	Biomass Producer Gas
SDG	Sustainable Development Goals
PM	Particulate Matter
LPG	Liquefied Petroleum Gas
US$	United States of America's Dollar [$]
GDP	Gross Domestic Product
1GS	First Generation Stoves
2GS	Second Generation Stoves
3GS	Third Generation Stoves
TSF	Traditional Three Stone Fire
PG	Producer Gas
SI	Spark Ignition
LBV	Laminar Burning Velocity [m/s]
CFD	Computational Fluid Dynamics
TLUD	Top-Lit Updraft Reactor
CVCB	Constant Volume Combustion Bomb
WBT	Water Boiling Test
LHV	Lower Heating Value [J/kg]

fuel under sustainability criteria, i.e. with higher efficiency, lower fuel consumption, and less pollutant emissions [5].

The development of improved cookstoves is grouped in three generations. The first generation stoves (1GS) are the plancha-type stoves based on combustion, whose efficiency reach values between 10% and 14% [6]. The second generation stoves (2GS) are the rocket-type stoves based on combustion, with efficiencies between 19% and 22% [7]. Among the third generation stoves (3GS), we found the gasification-based stoves, which reach efficiencies between 20% and 40% [8]. Furthermore, 3GS decrease the pollutant emissions of CO and PM by 50–80% and 65–95% respectively, with regard to traditional three stone fire (TSF) cookstoves [9,10]. The biomass energy-transformation process in the gasification-based cookstoves is composed by two stages. In the first stage is gasification the primary air (gasification-air) transforms the biomass in a gaseous fuel (biomass producer gas - BPG), and in the second stage, the Biomass Producer Gas (BPG) is oxidized in the combustion chamber with secondary air (combustion-air), where the thermal energy intended for cooking is released [11].

Laminar burning velocity (LBV) is an important property for assessing fuel combustion quality and modelling thermal engine processes. Many researchers have investigated the LBV of the main components of the BPG: methane, hydrogen, carbon monoxide and their mixtures. Reyes et al. [12] found that the laminar burning velocity in a spherical constant-volume combustion bomb of CH4-air was of 0.36 m/s, and 2.47 m/s for the H_2-air mixture. The H_2-air and H_2/CH_4-air mixtures reach a regime of cellular combustion characterized by the instability in the flame as a consequence of the expansion of the layer of unburned fuel close to the combustion bomb wall [13–15]. Wei et al. [16] analyzed the combined effects of H_2 and CO_2 in the LBV of the biogas and H_2 mixtures varying the CO_2 concentration in the biogas. A cylindrical combustion bomb combined with the Schlieren visualization technique was used. The reaction velocity decreased by 37% when CO_2 fraction increased from 40% to 60% in the biogas. This reduction was attributed to the thermal effects of CO_2 which reduce the adiabatic flame temperature, as well as the laminar burning velocity of the mixture. With regard to H_2 content increase in the mixture, the LBV increased due to a higher reaction rate [17], which was fostered by the kinetic and diffusion properties of H_2. And concerning to the flame front morphology, the flame stability decreased with the increase of H_2 in the mixture due to the thermal-diffusive and hydrodynamic instability. Nevertheless, when CO_2 content increased, the flame of the biogas-H_2 mixture tend to stabilize, which was attributed to the inhibition of the instability caused by the kinetic and thermal-diffusive properties of CO_2 [17].

Hernández et al. [18] compared the theoretical and experimental LBV of the BPG with *iso*-octane and CH_4 fuels under high initial pressure (50 bar) and high initial temperature (2300 K) conditions. The flame front velocity of the BPG (~5 m/s) is lower than that of *iso*-octane (~12 m/s), and slightly higher than that of CH_4 (3 m/s). The H_2 and CO concentrations in the BPG favored the increase of the adiabatic flame temperature, as well as the reaction rate and the burning velocity. Similar results were reported by Monteiro and Rouboa [11], who measured the LBV for three BPG derived from the most common gasification technologies, such as updraft (BPG heating value: 5.5 MJ/m^3), downdraft (5.7 MJ/m^3) and fluidized bed (5.4 MJ/m^3). The LBV decreased as the pressure increased from 0.5 up to 5.0 bar. An opposite trend was found for the LBV, which rose about 2.5 times as H_2 concentration increased from 9%vol up to 17%vol in the BPG. Andrade et al. [19] found that the LBV of the BPG (4.9 MJ/Nm^3) increased from 0.3 m/s to 0.33 m/s as a consequence of increasing the gas-air equivalence ratio from 0.85 to 1.0. These values were slightly below those reached by CH_4 (0.34–0.4 m/s) due to the presence of inert gases such as CO_2 and N_2 in the BPG. Nevertheless, the laminar burning velocity of the BPG is similar to that of liquid petroleum gas – LPG (0.33 m/s) under stoichiometric conditions for both fuels. This is due to the presence of H_2 in the BPG and its lower air requirements for the combustion process.

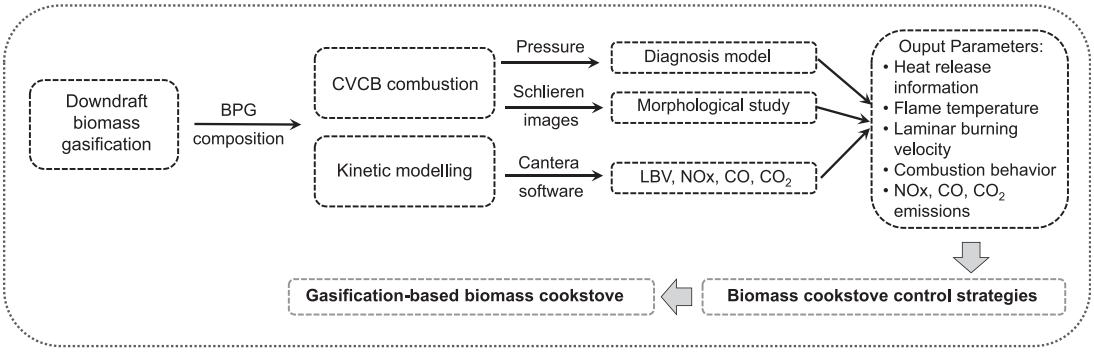

Fig. 1. Scheme of the methodology used in present work to characterize the BPG from a gasification based biomass cookstove.

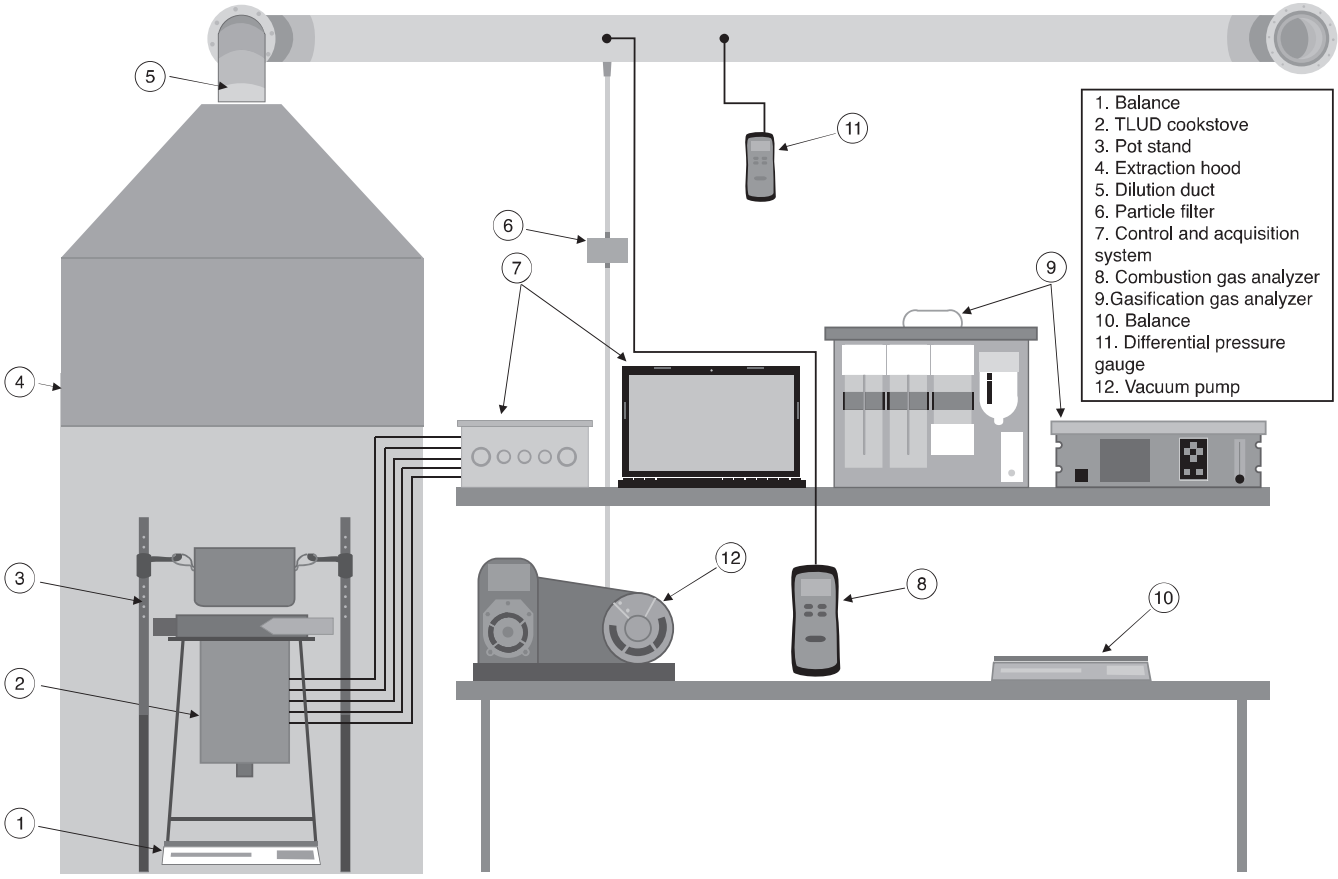

Fig. 2. Experimental facility of the gasification-based cookstove.

The BPG combustion has also been analyzed aiming to fuel SI combustion engines. Tinaut et al. [20] characterized the BPG combustion process in a constant-volume combustion bomb. The H_2 reduction in the BPG has a more noticeable effect in the burning velocity (which decreased from ~0.9 m/s down to ~0.5 m/s) than the CH_4 increase. Martínez et al. [21] investigated the syngas production in downdraft biomass gasifiers and its application using internal combustion engines. The effect of H_2 content is because its combustion velocity is of a higher order than that of CH4. Vieira Andrade et al. [19] studied the laminar burning velocity of BPG from Bunsen Burner methodology, and observed that fraction of hydrogen in the BPG influences the laminar burning velocity, and they used the Schlieren technique for flame visualization. Reyes et al. [22] found that the H_2 content accelerates the combustion process of H_2/CO mixtures. The mixtures with 0 and 6.7% of H_2 kept a laminar flame front even at the end of the combustion, while the mixtures with a high H_2 content (80%-100%) showed flame fronts with cellular surfaces. Teh et al. [23] investigated de combustion and emission characteristics of BPG in a combustion chamber for different biomasses and compared flame characteristics with those obtained for LPG.

Das et al. [24] evaluated the effect of steam addition in the LBV of a H_2-CO-N_2 mixture in an atmospheric counterflow burner. The flame laminar velocity decreased by 7.7% when the steam increased from 15% to 35%. This behavior is attributed to the higher specific heat of the water with regard to the other components of the reactive mixture. Whereby, the adiabatic flame temperature, as well as the LBV diminished. Hernández et al. [25] analyzed the effect of the BPG fraction in CH_4/BPG mixtures and the laminar burning velocity on NOx emissions from an atmospheric burner. As the BPG concentration increases (from 0% to 50%), the mixtures can be burned under fuel lean conditions. With

Table 1
Chemical composition of Patula pine and Cordia Alliodora wood chips.

Ultimate analysis dry-ash-free	*Pinus Patula*	*Cordia Alliodora*
C (wt %)	47.2	49.2
H (wt %)	6.2	5.8
N (wt %)	0.3	Not defined
O (wt %)	46.3	45.0
Proximate analysis		
Volatile matter (wt %)	84.11	81.75
Fixed carbon (wt %)	6.94	9.31
Ash (wt %)	0.4	1.53
Moisture (wt %)	8.55	7.41

Table 2
Average producer gas composition and wood gasification behavior for Patula pine wood chips and Cordia Alliodora.

Gasification parameters	*Pinus Patula*	*Cordia Alliodora*
Average maximum temperature (°C)	785.5	798.4
Biomass-air equivalence ratio (dimensionless)	2.75	2.69
Gasification reaction front velocity (mm/min)	11	12.1
Producer gas composition on dry base (vol%)		
CO	12.3	11.7
CO_2	15.4	15.9
CH_4	1.6	1.7
H_2	6.1	7.3
N_2	64.6	63.4
Low heating value LHV (MJ/Nm^3)	2.79	2.87

low gas-air ratios, the OH radical concentration significantly decreased due to a lower combustion temperature (main indicator of NOx formation). On the other hand, the LBV increased from 39 to 42 cm/s with the BPG concentration in the mixture, which resulted in a higher amount of air needed in the burner to stabilize the flame. Therefore, it was possible to work under fuel lean conditions, which led to decrease the NOx emissions, which is ascribed to the lower combustion temperature. By means of a theoretical analysis, Sukumaran et al. [26] developed a model of an atmospheric burner through CFD and kinetic chemistry, and found that, as NH_3 content increased in the BPG, the NOx emissions increased from 250 ppm to 700 ppm. This is attributed to the dissociation of NH_3 because it is the main source to produce NH and N_2. Serrano et al. [27] determined the LBV of a mixture of H_2, CO and N_2 considered as representative of the BPG, and experimentally studied the effects of flame stretch rate and instabilities in a constant volume combustion bomb and using CHEMKIN code.

Finally, Tryner et al. [28] assessed the combustion of a typical gas from a gasification-based cookstove (33% CO, 33% CO_2, 22% H_2, 7% CH_4, and 5% C_2H_4) through a non-premixed flame combustion chamber. As the air injection's velocity increased (8.8 m/s), its mixing with the gaseous fuel was fostered. The better mixing conditions favored a wider and more radiant heat release located under the height at which the air was injected. These results suggested that the low emissions (CO $\leq$ 8 g/MJ$_d$ and $PM_{2.5} \leq$ 41 mg/MJ$_d$) were found with higher combustion air velocities in the biomass gasification-based cookstove, which could be attributed to a better mixture between the air and the BPG. The reaction zone under the top section of the stove contributes to reduce the fuel-rich areas that foster the formation of soot and increases, as well, the time for CO and PM oxidation before the combustion gases heat the cold cooking surface.

The energy transition stage based in the supply of affordable and non-contaminating energy, including the population at risk in remote areas, requires clean fuels and/or electricity [1], as well as advanced biomass cookstoves with an adequate performance for the users, aiming to reduce the technical, social, and environmental impacts associated to biomass used as a cooking fuel [5,29,30]. In this work, the combustion of the BPG derived from a biomass gasification-based (or top lit up draft, TLUD) cookstove is studied in a constant-volume combustion bomb with a cylindrical geometry. The aim of this experimental and numerical work is to delve into the phenomenology associated with the BPG oxidation process as a function of controllable parameters such as the biomass type, initial temperature, initial pressure, and fuel/air equivalence ratio. Herein, it is assessed the effect on response variables such as burning velocity, pressure, flame front morphology, as well as calculated emissions of NOx, CO, and CO_2. The results found are intended to contribute to the development of cleaner gasification-based cookstoves, where the heat-release rate can promote a better energy and environmental performance.

2. Methodology

Fig. 1 shows a scheme of the methodology followed in this work. Initially, biomass is introduced in a biomass gasification process to obtain a biomass producer gas composition, which will be characterized in a constant volume combustion bomb and with a kinetic modelling to obtain parameters of interest during the combustion for future control strategies in the biomass cookstove development. The methodology carried out here could contribute to improve the control strategies of gasification-based cookstoves for increasing the efficiency and diminishing the pollutant emissions. The last two steps of Fig. 1 are out the scope of this work; nevertheless, in order to optimize the biomass gasification-based cookstoves, the main findings of this work could be implemented in future research.

2.1. Biomass gasification-based cookstove

Fig. 2 shows the outline of the experimental setup with its instrumentation, used to carry out the thermodynamic efficiency tests of the cookstove according to a modified water boiling test protocol (WBT 4.2.3), as well as the thermodynamic characterization of the gasification process [10]. The fundamental concepts of the biomass gasification-based cookstoves are described in Appendix 1.

The experimental tests in the cookstove were carried out with ~1300 g of biomass in the bed. For the biomass ignition, 3 ml of ethanol at 95% are added to the top of the cookstove. The cylindrical cookstove has an inner diameter of 0.16 m and a height of 0.28 m. The temperature in the gasification bed was measured by means of five K-type thermocouples, separated with a distance of 0.04 m from each other [31]. The biomass producer gas (or syngas) composition was measured by using a Gasboard-3100 Serial (Cubic-Ruiyi Instrument) gas analyzer. The composition of combustion gases was measured with a KIGAZ 310 (KIMO® Instruments) gas analyzer, and a K-type thermocouple measured the gas temperature. The experimental setup and the instrumentation used are presented in detail by Gutiérrez et al. [10].

Wood chips of *Pinus Patula* and *Cordia Alliodora* forest species were used as fuel in the cookstove, which are representative forest species planted in Colombia with potential as sustainable energy crops. The sizes of wood chips were between 4 and 20 mm with a bulk density of ~197 kg/m^3. The dry ash free ultimate analysis for both species is presented in Table 1 in terms of carbon, hydrogen, oxygen and nitrogen mass fractions, because sulphur were not detected [32].

The behavior of the forced-draft cookstove under the WBT 4.2.3 protocol using the wood chips as fuel reached a global thermal efficiency of 24.1%, while the specific emissions of carbon monoxide were of 2.75 g/MJ$_{delivered}$ [10]. The 3-stone cookfire had reached efficiencies between 11.83% and 14.9% [2,7,33], and specific emissions of carbon monoxide from 7.5 g/MJ$_{delivered}$ up to 15.1 g/MJ$_{delivered}$ [2,33]. Comparing the forced-draft cookstove with the three-stone cookfire, it is highlighted that the thermal efficiency of the former increases by ~79%, whilst the CO emissions diminishes by ~76%.

The better performance of the forced-draft cookstove against

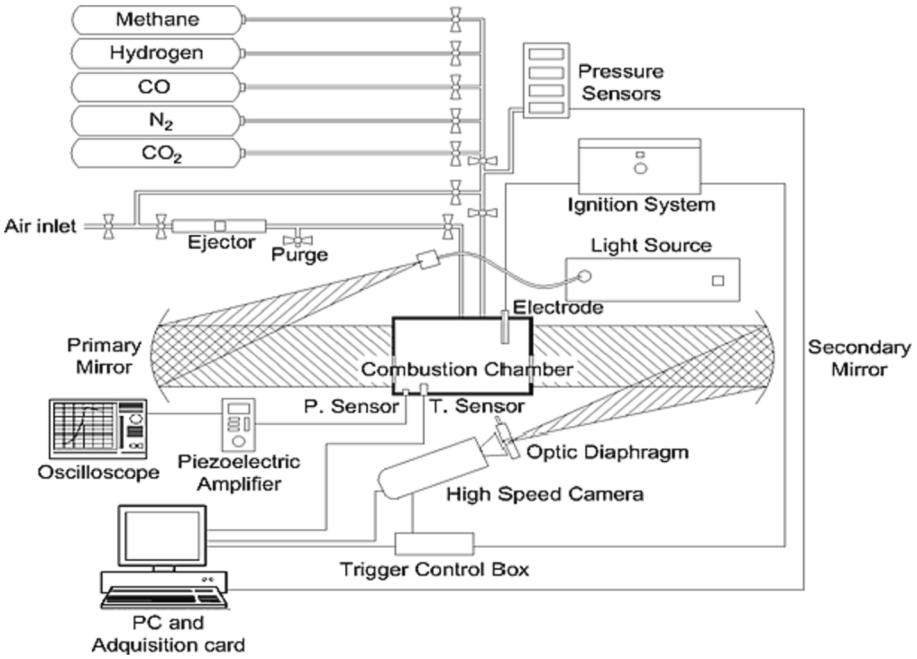

Fig. 3. Scheme of the experimental setup.

traditional cookstoves is ascribed to the two stages configuration for the biomass processing, biomass gasification and BPG combustion. The air forced draft contributes to improve two cookstoves characteristics. First, the gasification process is stable, and second, the combustion of BPG increases due to the mixing favored between the combustion air (oxygen) and the gaseous fuel. Therefore, the gasification-based cookstoves reach high efficiencies and low emissions [2,33]. In this work, the combustion of BPG is characterized seeking to understand and gain insight into the phenomenology of the oxidation of this gaseous fuel (with low calorific value), for contributing to improving the performance of forced-draft cookstoves in future works. Consequently, the input parameter for this work is the real BPG composition produced with wood chips in a gasification-based cookstove, see Table 2. The dry base BPG composition is shown in Table 2, the combustion behavior of this composition is assessed by a constant volume combustion bomb described in Section 2.2.

2.2. Experimental apparatus and procedure

2.2.1. Experimental setup: Constant volume combustion bomb

In this research work, the combustion of BPG mixtures are characterized in a cylindrical constant volume combustion bomb (CVCB) [14] for studying the burning velocity, rate of heat release, and burned mass fraction. The CVCB is a combustion chamber with cylindrical geometry with the following dimensions: diameter of 114 mm and 135 mm of length. This combustion bomb is used to investigate the combustion development under premixed conditions, see Fig. 3. The combustion chamber was designed with two optical windows made of fused silica on the sidewalls of the cylinder. The installation is instrumented to measure instantaneous pressure during the combustion process using a piezoelectric pressure transducer Kistler type 7063.The installation is also prepared to register the flame development with a high-speed Schlieren photography system: flame images were recorded using a high-speed camera Phantom V210 at 7000 frames per second (resolution 832 × 800 and exposure time of 10 ms).

Gaseous fuels and air are individually introduced from pressure tanks using partial pressure method, and an ignition system starts the combustion at the center of the combustion chamber. At the start of each combustion process, the initial conditions of pressure, temperature and fuel/air equivalence ratio are set up. The BPG composition is introduced into the CVCB with the corresponding amount of the air, and initial conditions of pressure and temperature. Once the combustion is initiated, a spherical flame front is propagated inside the CVCB, while the fresh mixture is compressed and burned.

2.2.2. Image processing

A home-developed algorithm is used to process the images obtained with the Schlieren technique (high-speed camera), for determining the time evolution of the flame radius and to study the cellular structure which appears as a wrinkling of the flame surface. Radius evolution is analyzed through frame by frame processing, after background removal, binarization and thinning transformation to highlight the borders between cells, as it is explained in detail by Tinaut et al. [14]; where the image processing allows to find the instantaneous position of the flame front (with a random sample consensus algorithm programmed in Matlab) and identifying the cells that appear in the flame during de combustion development.

Flame propagation speed (*Sn*) can be determined from the flame front radius, as shown in Eq. (1).

$$Sn = dR/dt \tag{1}$$

The stretched burning velocity (u_n) is derived from the flame propagation speed by considering the mass conservation in the flame front, Eq. (2).

$$u_n = (\rho_b/\rho_u) \bullet S_n \tag{2}$$

where ρ_b and ρ_u are the densities of the burned and unburned zones [14]. Furthermore, the laminar burning velocity (u_l) can be calculated considering the expanding rate of the flame front area due to aerodynamic strain with the Stretch rate.

$$u_l - u_n = L\alpha \tag{3}$$

where L is the Markstein length, and α the Stretch rate, Eq. (4).

$$\alpha = \frac{1}{A_f}\frac{dA_f}{dt} = \frac{2}{R}\frac{dR}{dt} = \frac{2}{R}S_n. \tag{4}$$

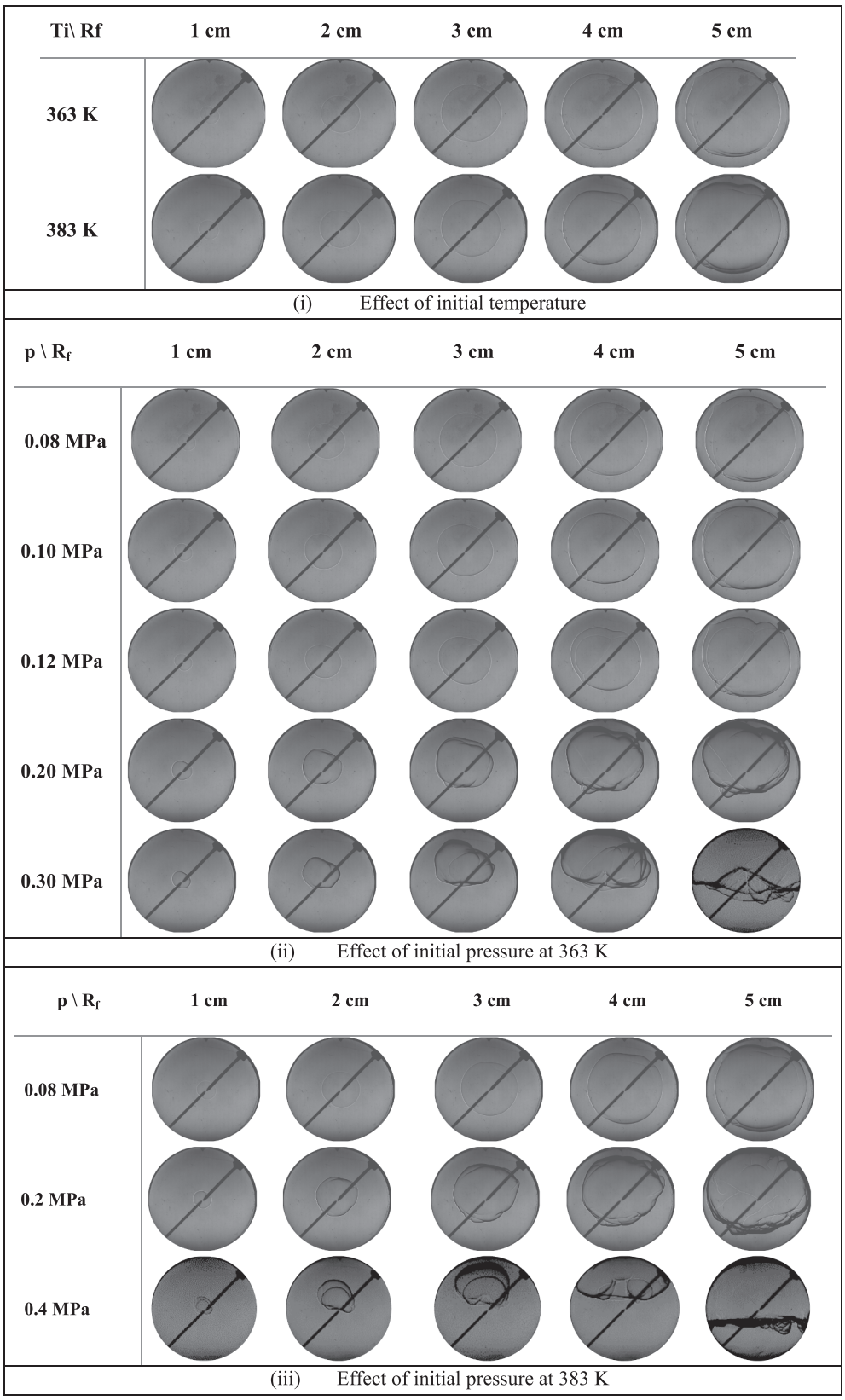

Fig. 4. Schlieren images for Pinus Patula BPG stoichiometric flames.

2.2.3. Two-zone thermodynamic model

The outputs of the model are the LBV, combustion temperature, and mass fraction. Pressure signal is taken as an input parameter in the two-zone thermodynamic diagnosis model, which considers the division of the combustion chamber into two zones, burned and unburned, and the application of thermodynamic laws, energy, mass, and volume conservation, considering ideal gas behavior to both zones [15]. With the thermodynamical diagnosis model, it is possible to determine some

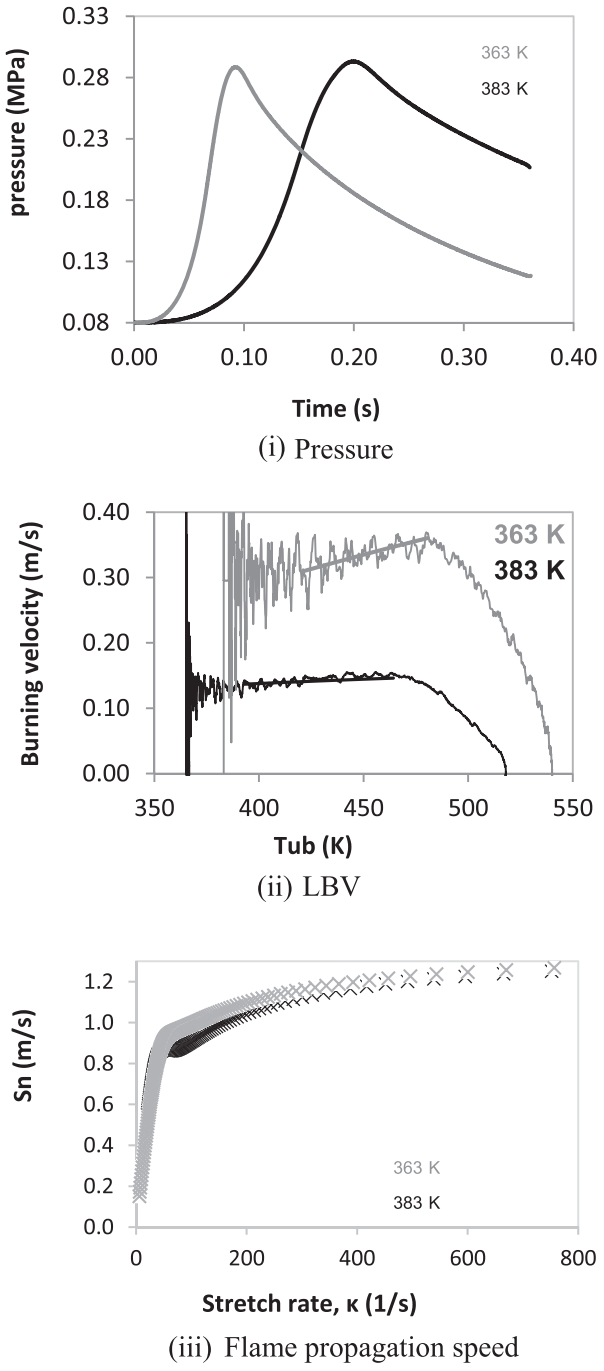

Fig. 5. Pinus Patula BPG flames for stoichiometric conditions and 0.08 MPa of initial pressure.

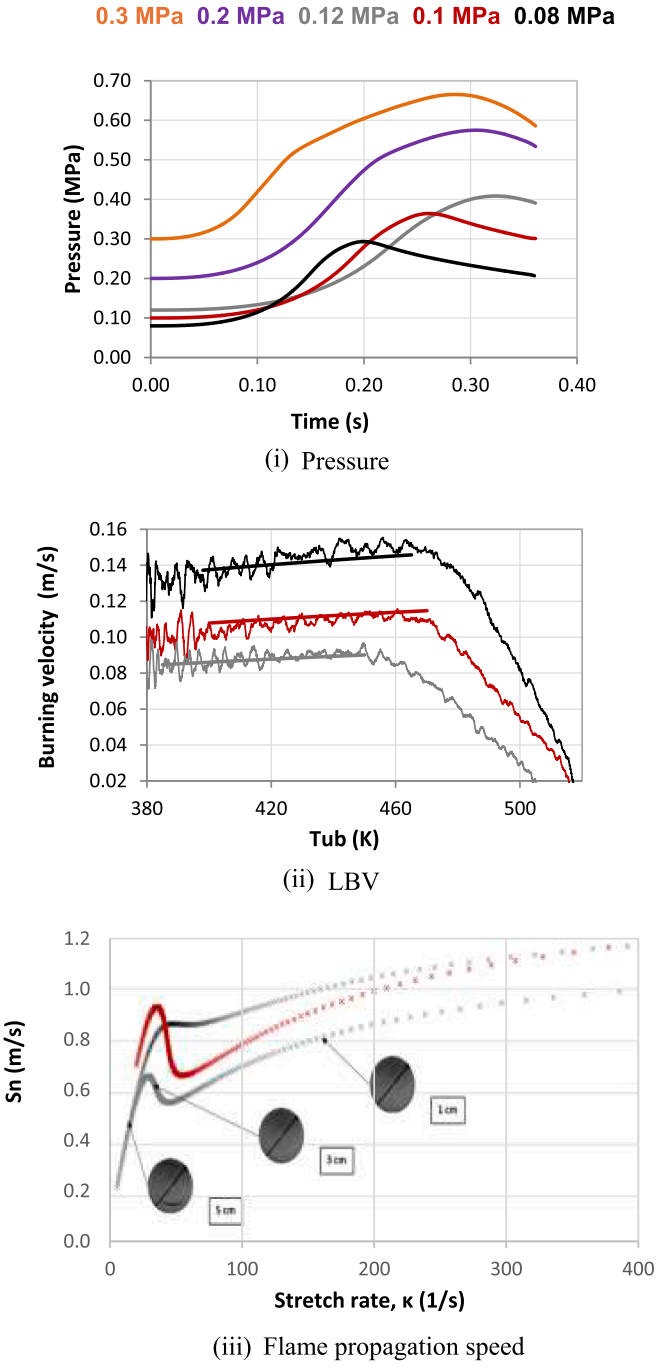

Fig. 6. Pinus Patula BPG flames for stoichiometric conditions and 363 K of initial temperature.

parameters to characterize the combustion process such as the unburned temperature, adiabatic flame temperature, rate of heat release, burned mass fraction, and laminar burning velocity. The laminar burning velocity (u_l^p) is calculated from the mass burning rate $\dot{m}_b$, the unburned mixture density ρ_b, and the flame front surface (A_f), according to Eq. (5).

$$u_l^p = \dot{m}_b / \rho_b A_f \tag{5}$$

2.2.4. Kinetic modelling using Cantera

A kinetic study of the BPG combustion contributes to interpret and explain the experimental results, to obtain the chemical species during the combustion process, and to understand the chemical and physical phenomena that take place during the combustion process. Kinetic combustion modelling includes the resolution of a differential equations system with elevated computational charge. Nowadays, there are tools, based on computational codes, that includes reaction mechanisms to find consistent theoretical solutions to combustion problems. In this work is used Cantera software [34] with the GRI-Mech 3.0 [35] kinetic

Table 3
Values of the coefficients for the correlation presented in Eq. (6).

$u_{l,0(\frac{m}{s})}$	α	β	R^2
0.0377	4.978	−1.239	0.981

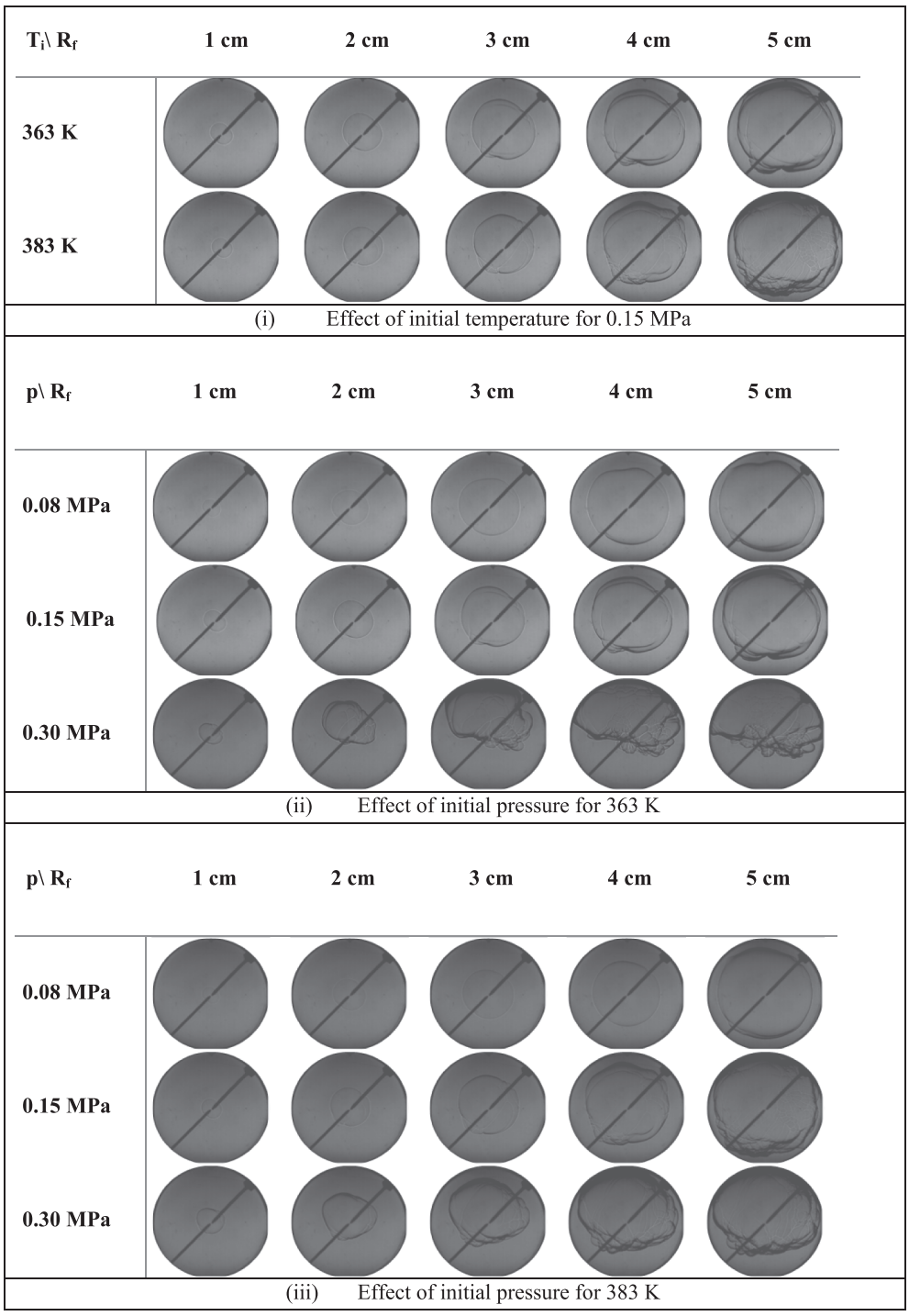

Fig. 7. Schlieren images for Cordia Alliodora BPG stoichiometric flames.

reaction mechanism accepted for BPG components, which consists of 325 elementary chemical reactions and 53 species. Besides, it has been use Aramco 1.3 kinetic mechanism [36] to compare LBV and flame temperature results with GriMech 3.0. By using Cantera and GriMech the emissions of NO, NO_2, CO, and CO_2 are calculated. These combustion parameters are important due to their effect on the environment and on people's health.

3. Results and discussion

The results of this work are classified in two sections, since the experimental and numerical viewpoint. First, biomass producer gas compositions (for Pinus Patula and Cordia Alliodora) are characterized in the cylindrical CVCB for assessing the effect of composition, initial temperature, and pressure on the combustion process by parameters, such as burning velocity, flame propagation speed, and flame morphology. Second, by using Cantera kinetic model with Gri-Mech 3.0 mechanism, parameters such as laminar burning velocity, flame temperature, and NOx, CO, CO_2 emissions from the BPG compositions are calculated.

3.1. Characterization of Pinus Patula BPG in the cylindrical CVCB

In this section, the combustion results of Pinus Patula BPG as a

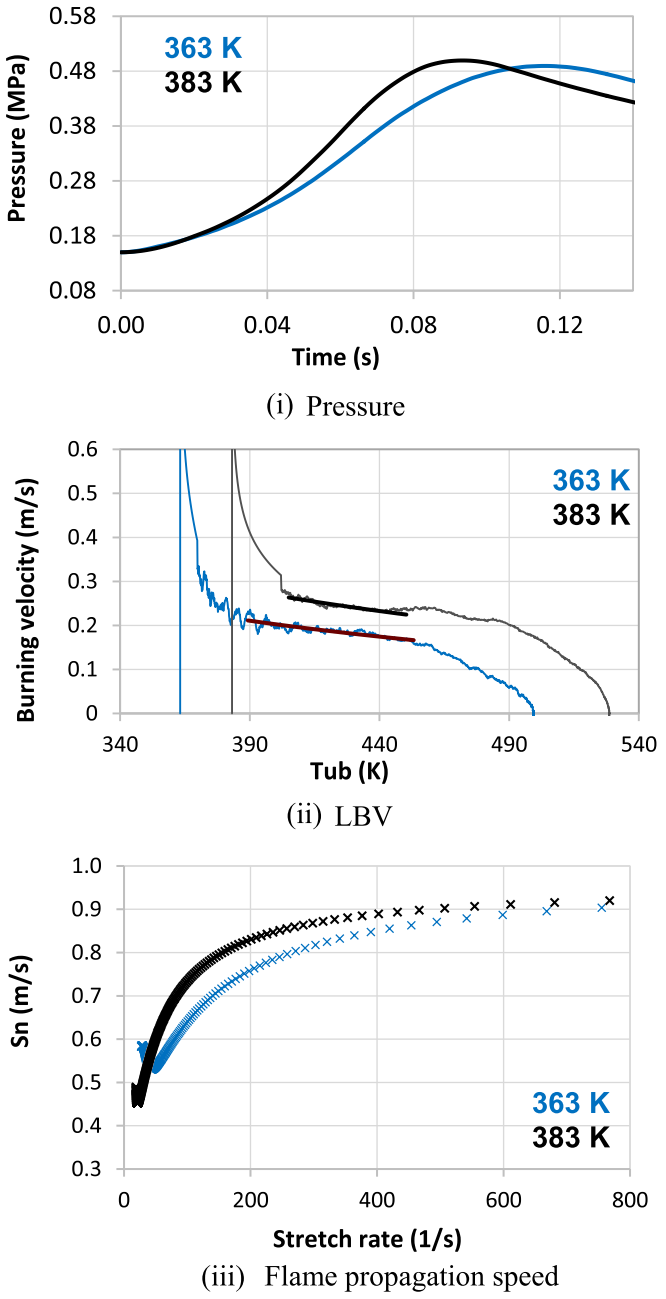

Fig. 8. Cordia Alliodora BPG flames for stoichiometric conditions and 0.15 MPa of initial pressure.

function of initial temperature and pressure on the burning velocity, and flame morphology that is characterized by flame instabilities, under stoichiometric fuel-BPG /air equivalence ratio conditions are presented.

3.1.1. *Flame front morphology*

In this study, the effect of initial temperature and pressure on the flame front morphology of Pinus Patula BPG is investigated. Schlieren images for Pinus Patula BPG mixture under stoichiometric conditions, setting the initial pressure at 0.08 MPa, and varying the initial temperature (363 K and 383 K) are presented in Fig. 4i. In that Figure, it is possible to see that at the beginning, the spark plug originates a combustion kernel which propagates spherically outwards, increasing the instantaneous pressure inside the CVCB. The flame front grows spherically outwardly until it collides with the walls of the CVCB. The flame front is laminar, and it is considered stable in both cases, because it does not develop a cellular flame front but only presents some wrinkles in the last phase of the combustion, mainly due to the electrodes effect and buoyancy phenomenon. The combustion stability and the flame front structure and wrinkling is defined by the instabilities growth rate in the first stages of the combustion. There are three phenomena that contribute to the instability development in the flame front of a premixed combustion: hydrodynamic effects (destabilizing) associated with the density difference between the unburned and burned mixtures; thermo-diffusive effect (destabilizing or stabilizing, depending on the nature of the combustion) linked with the thermal and molecular diffusivity; and volume forces related with the buoyancy (generates wrinkles related to the gravity force) [13]. During the spherically grown, the hydrodynamic effect has always a destabilizing character. Meanwhile the thermal-diffusive and stretch effects stabilizes the hydrodynamic and flame stretch effects. Therefore, a laminar flame front is obtained as it is presented in Fig. 4i [13], i.e. without a cellular structure.

Fig. 4ii shows Schlieren images of Pinus Patula flame evolution during combustion for different radius, varying the initial pressure from 0.08 MPa up to 0.3 MPa, for an initial temperature of 363 K, and form 0.08 MPa to 0.4 MPa, for an initial temperature of 383 K. At first sight, it can be noticed that experiments for lower initial pressures (0.08–0.12 MPa) achieve a centered flame which grows spherically until it reached out the CVCB walls. For higher initial pressures (0.2, 0.3, and 0.4 MPa) for both temperatures, it is possible to see a different behavior since the flame front is not centered, and it moves away from the combustion bomb center with an upward trend due to the buoyancy phenomena. For the high initial pressures, flame front is not spherical; thereby, the hypothesis of the two-zone thermodynamic model cannot be applied.

Effects of gravity on the flame propagation come to be important in flames with low burning velocities, for example those with lean mixtures or high initial pressure. Due to the difference on temperature between the burned and unburned mixtures, a buoyancy force causes the increment of the burned mixture. For spherical flames, this phenomenon causes upward displacement of the flame kernel, so that the flame reaches the top of the vessel earlier, increasing the heat transfer with the CVCB walls. Cracks are formed in the flame front for higher initial pressures (0.2–0.3 MPa) because the thermal-diffusive effect cannot stabilize the hydrodynamic effect, and due to the volume forces effect, that is the buoyancy phenomenon. The effect of initial pressure can also be studied in Fig. 4iii where Schlieren images are presented for stoichiometric Pinus Patula BPG flames with initial temperature of 383 K and initial pressures of 0.08, 0.2 and 0.4 MPa. As can be seen, only the flame front for 0.08 MPa is spherical. For higher initial pressures, buoyancy effect is important because of the deformation on the flame front. In those cases, as commented above, it is not possible to use the two-zone thermodynamic model because of the lack of the sphericity hypothesis in the flame front that avoids reading the flame radius from images.

3.1.2. *Effect of initial temperature and pressure*

Herein is assessed the effect of initial temperature and pressure on instantaneous pressure register and burning velocity for outwardly propagating spherical laminar Pinus Patula BPG flames.

Initially is studied the effect of varying initial temperature by representing in Fig. 5i instantaneous pressure evolution of the corresponding mixtures caused by the outwardly flame front propagation, setting the initial pressure at 0.08 MPa, and varying the initial temperature from 363 K and 383 K, where it is possible to see an increment in the pressure curve until the maximum value is reached at the end of the combustion, decreasing afterwards due to heat transmission. The increment on initial temperature elevates the adiabatic flame temperature, which accelerates the combustion reaction rates and the laminar burning velocity of the fuel–air mixture as it is presented in Fig. 5ii, where the burning velocity (u_l^p) is depicted versus the unburned temperature, for the two initial temperatures considered.

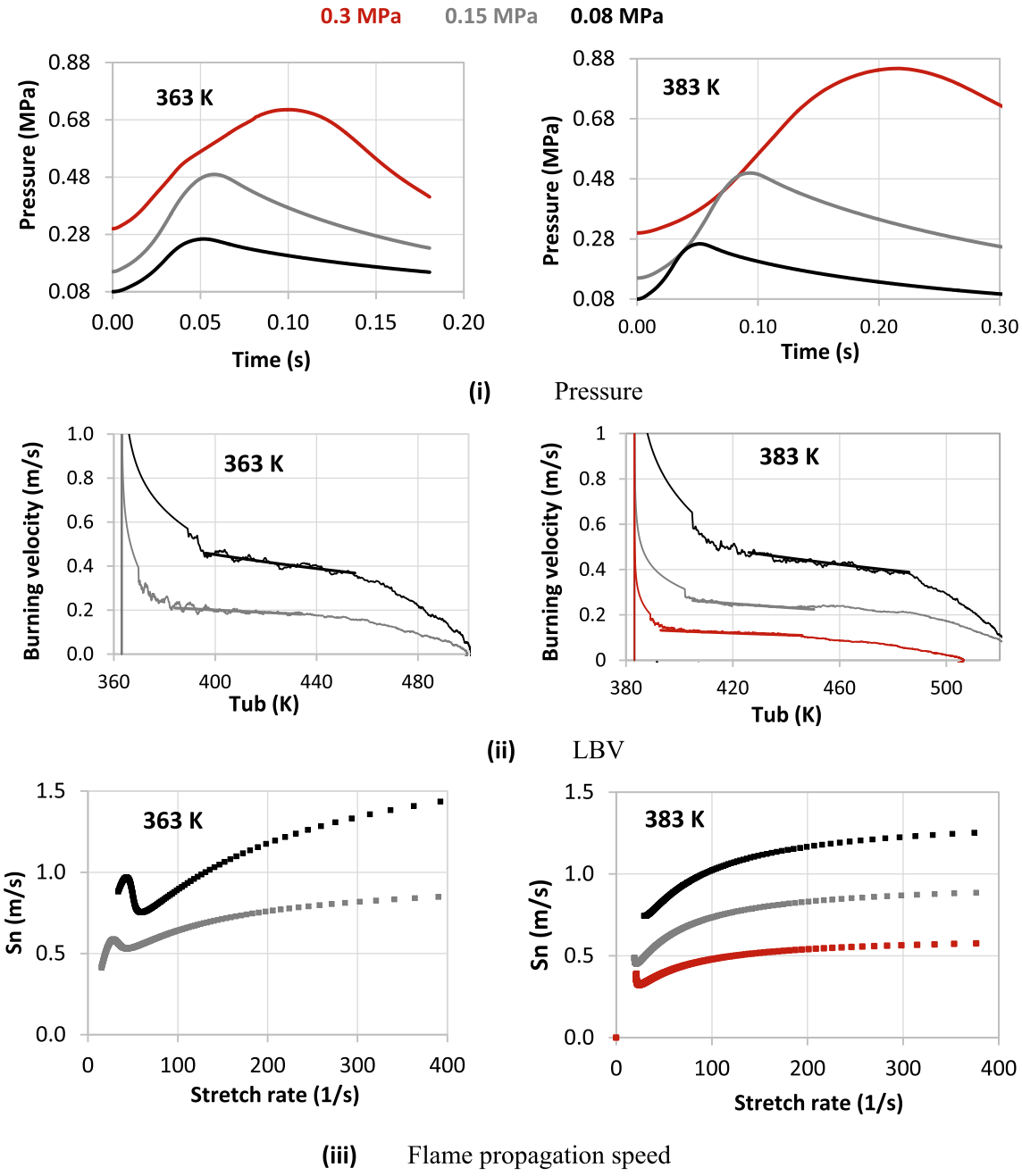

Fig. 9. Cordia Alliodora BPG stoichiometric flames.

Table 4
Values of the coefficients for the correlation presented in Eq. (6) for Cordia Alliodora.

$u_{l,0}$	α	β	R^2
0.21064	3.17043	−1.2786	0.994

Simultaneously, it is possible to obtain the evolution of the flame radius during the combustion process, determined by the Schlieren images and the flame propagation speed (*Sn*) versus the stretch rate, presented in Fig. 5iii. Notice that the stretch rate is high at the beginning of the combustion due to the curvature of the flame. Nevertheless, the stretch rate decreases with the flame radius, which means in Fig. 5iii, that the combustion origin is on the right part. Flame propagation speed gradually decreases as the Strech rate declines.

The effect of initial pressure is analyzed in Fig. 6, where Pinus Patula BPG flames evolution during combustion are presented varying the initial pressure from 0.08 MPa up to 0.3 MPa, for an initial temperature of 363 K. Pressure evolution is plotted in Fig. 6i, where it is noticeable the difference between the shape of the high initial pressure curves (blue and purple, 0.3 and 0.2 MPa, respectively) and the low initial pressure curves (black, red, and grey). For low initial pressures (0.08–0.12 MPa) the curves show the same shape of the ones presented in Fig. 5i. However, for high initial pressures, it can be observed the consequences of the buoyancy phenomenon detailed in previous section, which shows a decrease in the rate between peak and initial pressure for the combustion processes with higher initial pressures (0.2 MPa and 0.3 MPa) compared to those with lower pressures. Only curves for low initial pressure are analyzed with the thermodynamic model, and results of burning velocity versus unburned temperature are presented in Fig. 6ii. It is worth note a negative effect of the initial pressure on the burning

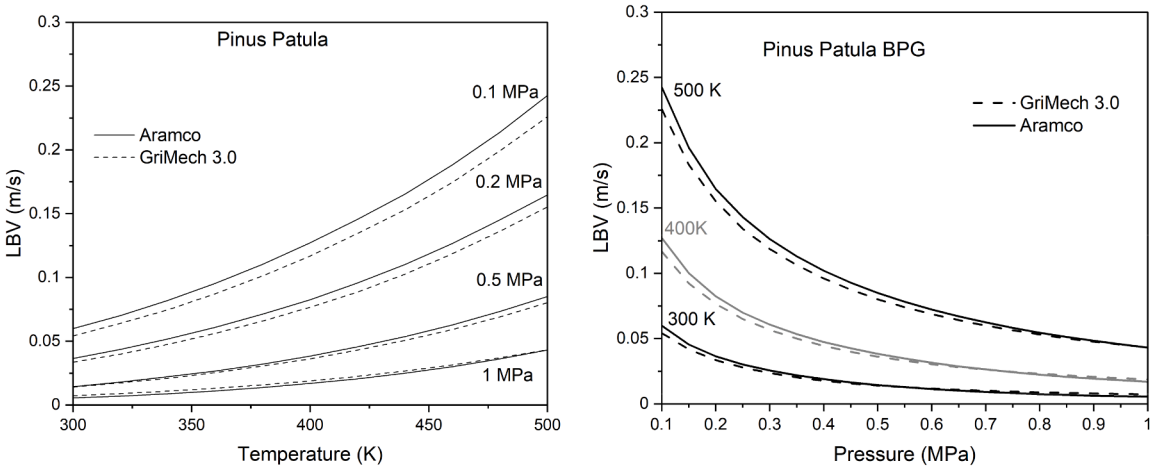

(i) LBV versus temperature and pressure for Pinus Patula BPG stoichiometric mixtures

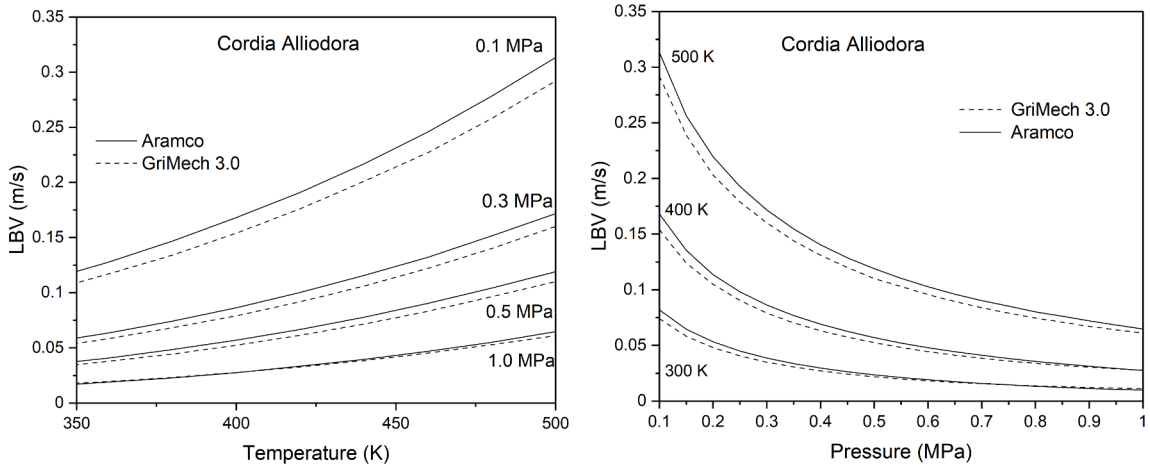

(ii) LBV versus temperature and pressure for Cordia Allidora BPG stoichiometric mixtures

Fig. 10. Comparison of LBV results calculated with GriMech 3.0 and Aramco kinetic mechanisms.

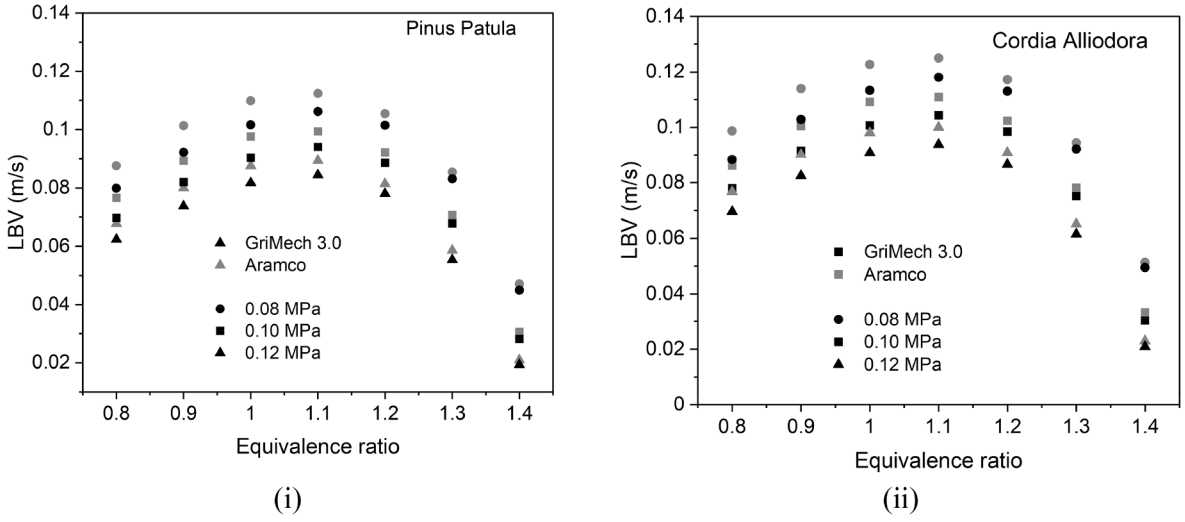

Fig. 11. Laminar burning velocity of BPG versus equivalence ratio for 363 K of initial temperature.

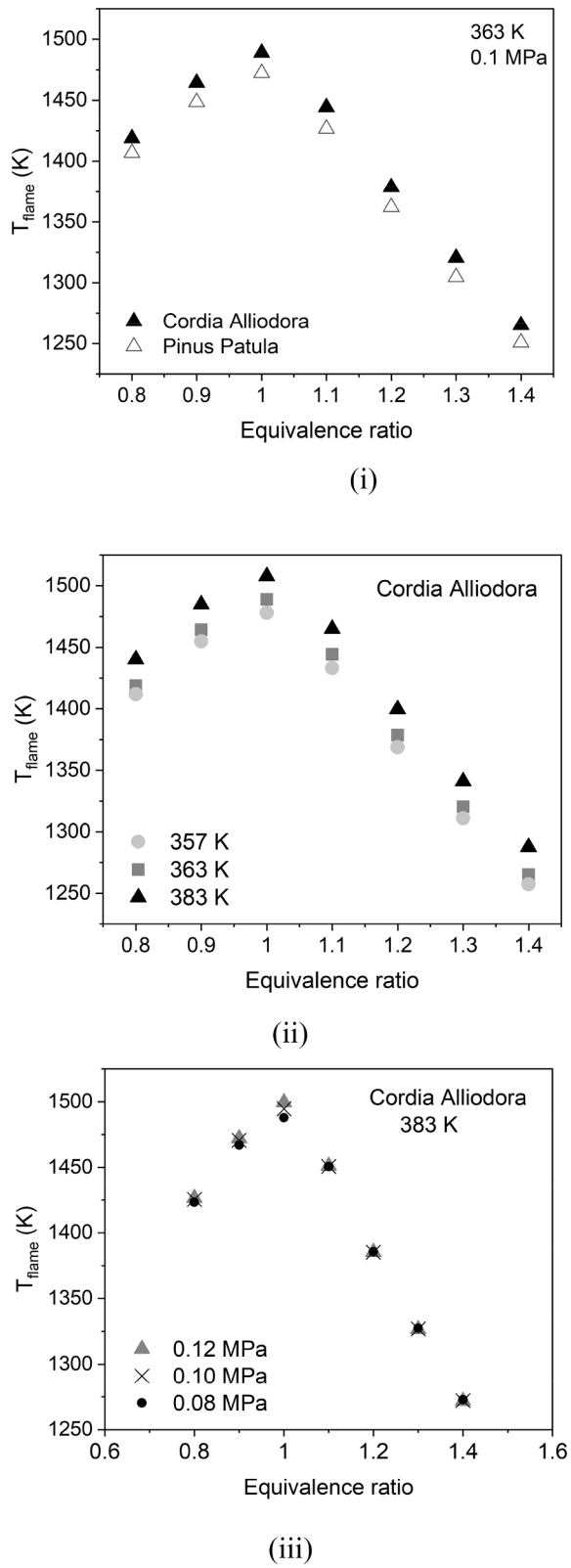

Fig. 12. Flame temperature versus fuel/air equivalence ratio for (i) Different BPG compositions, (ii) Effect of initial temperature Cordia Alliodora, (iii) Effect of initial pressure.

velocity, since as the initial pressure increases, the burning velocity diminishes. The inverse dependence of the laminar burning velocity with pressure is ascribed to the fact that the mass burning rate is proportional to the square root of the global reaction rate [37,38].

Oscillations shown in Fig. 6ii, that appear at the beginning of the combustion, are due to the ignition process by using a spark. Therefore, the curve grows until it reaches the maximum velocity that matches with the instant at which the maximum pressure was reached. So, the pressure decreases when the combustion ends. Only experiments with spherical flame front are considered for determining the burning velocity. Therefore, only environments with zero-gravity will eliminate the upwards movement of the flame front and the buoyancy effects [39]. Burning velocity can be adjusted by means of a multilinear regression Metghalchi and Keck type [40] according to Eq. (6).

$$u_l^p(m/s) = u_{l0}\left(\frac{T}{T_0}\right)^{\alpha}\left(\frac{p}{p_0}\right)^{\beta} \tag{6}$$

where u_l^p is the burning velocity and u_{l0} is the laminar burning velocity at the reference conditions (T_0 and p_0, normally considering 300 K and 0.1 MPa, respectively). The temperature exponent, α presents positive and higher values between $1 < \alpha < 2.5$ for the most common fuels and its value depends on the type of mixture and the fuel/air ratio. The pressure exponent, β usually presents negative and lower values between $-0.5 < \beta < 0$ and it also depends on the type of fuel/air mixture and fuel/air ratio. The values obtained for the data represented in Fig. 6, for pressures between 0.08 MPa and 0.4 MPa and temperatures from 360 K to 520 K, are those presented in Table 3.

Results of propagation speed using Schlieren optical technique, for low initial pressure, stoichiometric conditions with an initial temperature of 363 K, are presented in Fig. 6iii, reads from right to left, since the combustion beginning presents higher stretch rates (as the curvature is more elevated and the radius is smaller); whilst the combustion end presents lower stretch rates. Some images are inserted in Fig. 6iii to see the morphology of the flame at this time. Spherically propagating flame is subjected to the flame stretch due to the curvature of the flame front. And its burning velocity varies accompanied with the change in the curvature during the explosion expressed by the Stretch rate defined in Eq. (4).

3.2. Characterization of Cordia Alliodora BPG in the cylindrical CVCB

Herein, it is presented an experimental study of the stoichiometric combustion of the BPG corresponding to the Cordia Alliodora forest species as a function of initial temperature and pressure.

3.2.1. Flame front morphology characterization

Schlieren images combustion of Cordia Alliodora BPG at different flame radius are presented in Fig. 7. The effect of initial temperature and pressure on flame morphology is studied here. Some wrinkles appear in the flame front, which could be ascribed to the instabilities in the flame front that modifies the flame morphology with the apparition of a cellular structure. The wrinkles appear in the flames for both temperatures, however they are more protuberant in the flames for the highest initial temperature (383 K), where the beginning of a cellular structure can be observed. In Pinus Patula BPG flames these instabilities appear but not modify the flame front morphology due to the stabilizing thermal-diffusive effect. However, in Cordia Alliodora BPG flames, the instability growth rate is positive because some cells and wrinkles appear in the flame. that means, that during the spherically grown the stabilizing thermal-diffusive effect could not stabilize hydrodynamic effect, whereby a cellular structure is obtained, as can be seen in Fig. 7i for 383 K.

In Fig. 7ii and 7iii Schlieren images for Cordia Alliodora stoichiometric flames are presented for an initial temperature set at 363 K and 383 K, respectively, varying the initial pressure. The increase on the

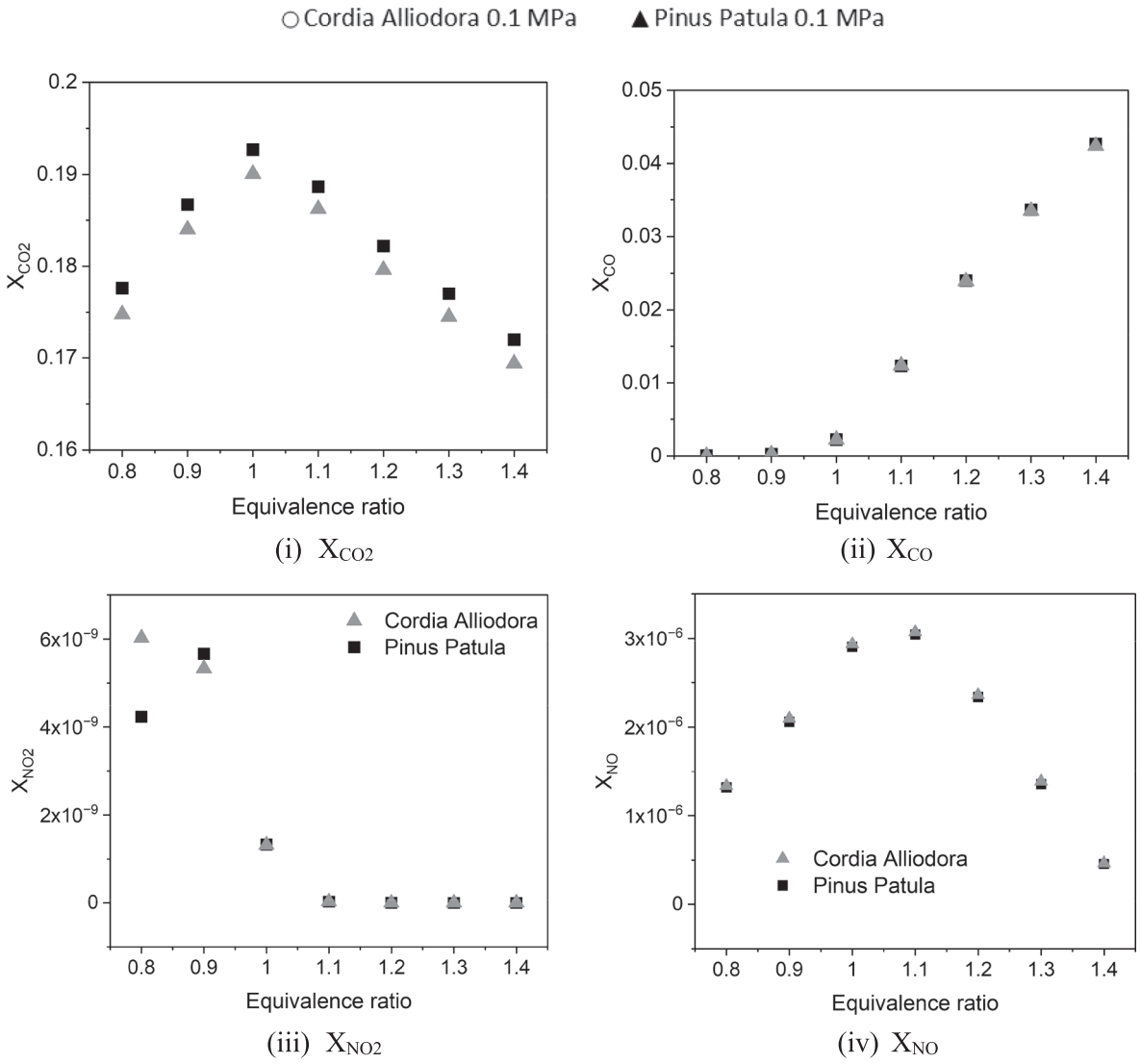

Fig. 13. Molar fraction of CO, CO_2, NO_2 and NO emissions for Pinus Patula and Cordia Alliodora BPG compositions at 365 K of initial temperature, 0.1 MPa of initial pressure versus fuel/air equivalence ratios.

buoyancy with the initial pressure can be notice in those Schlieren images, which produces the non-sphericity of the flame front, and the development of cells and wrinkles on it, which leads to a wrinkled structure for elevated radius in the cases of initial temperature at 383 K, where the thermal-diffusive effect cannot stabilize the hydrodynamic effect, thereby, a cellular structure is reached (Fig. 7iii).

3.2.2. *Effect of initial pressure and temperature*

The influence of initial pressure and temperature on experimental results such as the instantaneous pressure inside the combustion bomb, the burning velocity calculated by a diagnosis model, and the flame propagation speed are presented in this section.

Pressure evolution, burning velocity, flame radius and flame propagation speed are presented in Figs. 8 and 9. It can be seen that the initial temperature accelerates the flame due to the increment on the combustion rate, and displace the peak pressure to a lower time, as it was expected. The flame propagation speed shows different patterns depending on the initial temperature and pressure. Fig. 9iii shows the change in the flame propagation speed due to the apparition of cracks in the flame. For high stretch rates (low radius at the beginning of the combustion) the influence of temperature is not significant on the propagation speed, but, as the combustion progresses, the effect of the initial temperature becomes more important (see Fig. 9iii).

As the initial pressure increases, the combustion duration rises and the peak pressure is displaced to higher times; therefore, the burning velocity and flame front propagation speed diminish, as it happened with the Pinus Patula BPG, see Figs. 5 and 6.

The influence of initial pressure on Cordia Alliodora BPG flames for high temperatures is depicted in Fig. 9iii, according to Schlieren images of the combustion at different radius, for 383 K of initial temperature and various initial pressures that have been presented in Fig. 9i. It is possible to see an increment on the buoyancy effect with the increment of the initial pressure. As the pressure increases, the morphology of the flame front changes (see Fig. 9i), appearing some wrinkles which makes a wrinkled flame front. The effect of the increment in pressure is the same than the observed for 363 K, showing an inverse effect on the burning velocity and flame front propagation speed.

To summarize, it is possible to state that the increment in initial temperature accelerates the flame, and it is reflected in an increment in the burning velocity and flame propagation speed due to the combustion rate. But, on the other hand, the effect on the increment in the initial pressure is the opposite. The coefficients of the Metgalchi and Keck correlation obtained for Cordia Alliodora BPG flames are detailed in Table 4.

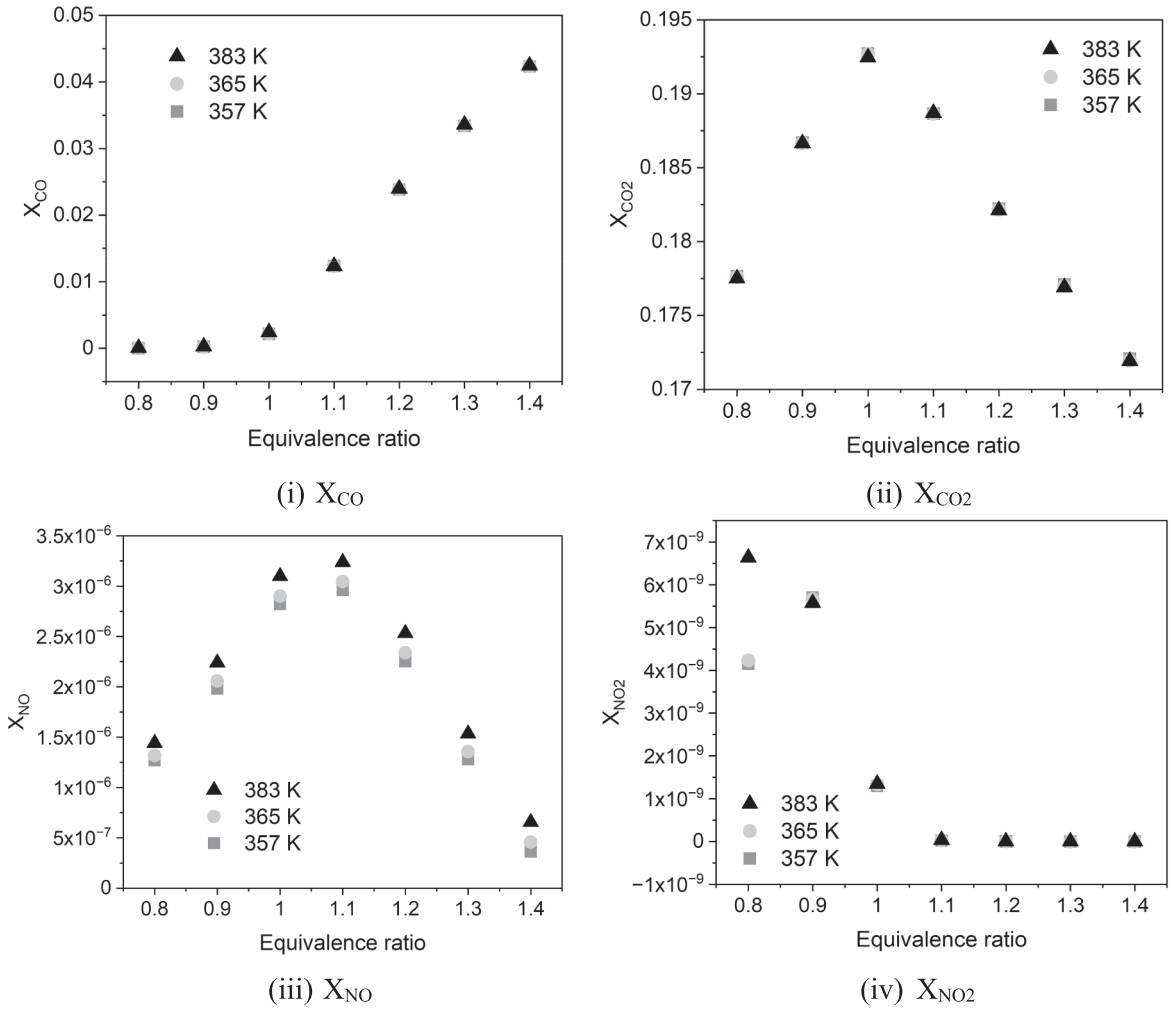

Fig. 14. Molar fraction of NOx, CO and CO_2 emissions from Pinus Patula BPG composition for 0.1 MPa versus initial temperature and gas/air equivalence ratio.

3.3. Kinetic modelling results

The combustion process analyzed by a kinetic approach allows to understand the physical and chemical phenomena that take place inside the combustion bomb, and to interpretate experimental results. There are computational codes that use reaction mechanisms for combustion modelling and obtain theoretical solutions of combustion problems. Here, the tool Cantera [34] is used, with the kinetic reaction mechanism GRI-Mech 3.0 [35] and Aramco [36,41]. Fig. 10 shows the results obtained with the two chosen mechanisms, Aramco mechanism reaches slightly higher values of the LBV than GriMech, whose average difference is about 7% (6% for the lower pressures of 0.1 MPa, and 8% for initial temperatures of 500 K).

Results of the laminar burning velocity obtained with GriMech 3.0 and Aramco for BPG of Pinus Patula and Cordia Alliodora are presented in Fig. 11i and 11ii, respectively, for different fuel/air equivalence ratios, with an initial temperature of 363 K. Fig. 11 shows that the laminar burning velocity of Cordia Alliodora is higher than that of Pinus Patula for all the initial pressure conditions considered (10.8% more for 0.12 and 0.1 MPa, and 11.1% for 0.08 MPa initial pressure conditions). Zhou et al.[42] determined that, a gas mixture composed of H_2, CO and CH_4, a higher percentage of H_2 significantly contributed to the increase of the laminar combustion velocity of the mixture. In this same type of mixtures, the increase of CH_4 had a negative influence on the combustion velocity. Lafuente [43] carried out a statistical study showing the influence of the concentrations of the different gases on the laminar combustion velocity. By means of a Pareto diagram, this author concluded that the component that most influences the rise in the combustion velocity of the mixture is H_2. CH_4 is the second most influential component, but the CH4 affects in a negative way, i.e., an increase in its concentration in the mixture gas leads to a decrease in the LBV. According to Lafuente, the percentage of the CO has a positive influence on the LBV of the BPG, although its influence is less than that of CH_4 and, especially, much less than that of H_2. Alternatively, Zhou et al. [42] maintain that the influence of the CO is practically nil. The inert gases, both CO_2 and N_2, slow down all the kinetic processes and thus the rate LBV of the combustions process [44]. Finally, Lafuente determined that, although in a much less influential way, the interrelationship between CH4 and H2 influences negatively in the LBV of the BPG. The latter is explained taking into account the research conducted by Vagelopoulos et al. [45] and by Scholte et al. [46], since CH_4 slows H_2 not linearly, but quadratically.

Considering the latter, it is observed that Cordia Alliodora has 1.2% more H_2 in the BPG mixture than the Pinus Patula BPG mixture. As it was explained before, the H_2 percentage is the most influential parameter in the LBV, thus this fact shows the main reason why the speeds are different. The N_2 percentage is another factor that affects to the LBV, being this one higher in Pinus Patula than in Cordia Alliodora. As indicated, being an inert, N_2 slows down the kinetics of combustion. The proportion of CH_4 in both mixtures is very similar, therefore, it is not considered as a significant compound for the difference in the LBV in this case. Although the BPG from Cordia Alliodora has a higher proportion of CO_2 and a lower proportion of CO compared to that from Pinus Patula, the difference and influence between these two

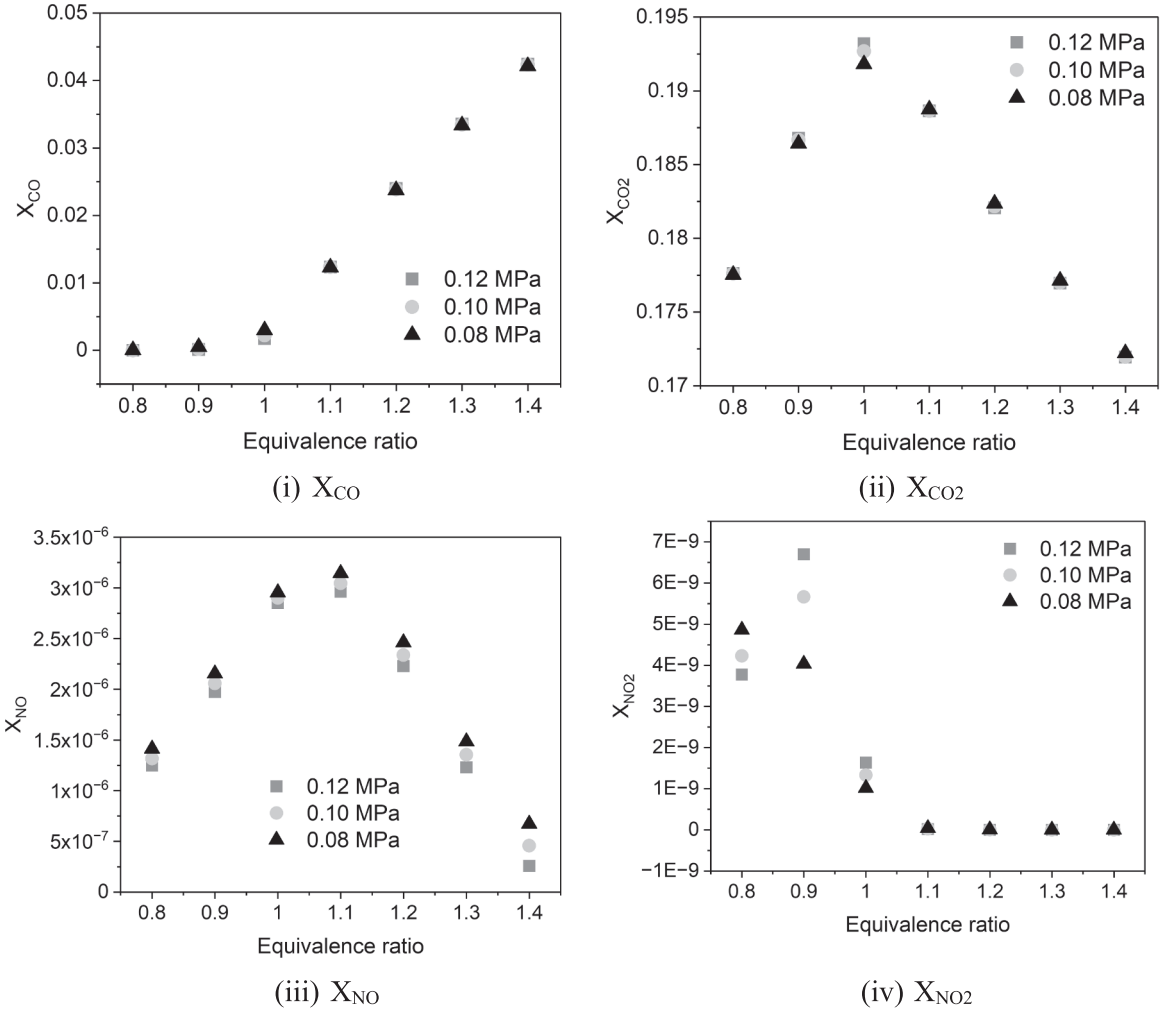

Fig. 15. Molar fraction of NOx, CO and CO2 emissions for Pinus Patula BPG composition for 383 K versus initial pressure and equivalence ratio.

compounds in this mixture is smaller than the H_2 effect described above. It is concluded, therefore, that the difference between the two rates is due, above all, to the difference in the percentage of H_2 and a little to the difference in the percentage of inert species between the BPG mixtures.

The compositions of Pinus Patula and Cordia Alliodora are different, which makes that the chemical kinetic is different. The main difference is the percentage of H_2 in the fuel mixture, Cordia Alliodora has 1.2% of H_2 more than Pinus Patula. Taking into account the high burning velocity of H_2, 3.976 m/s for the conditions of 362 K and 0.4 MPa, and stoichiometric equivalence ratio, we obtained a value of 0.265 m/s for the same conditions of Pinus Patula, which means that the H_2 velocity is 15 times higher than that of the producer gas assessed here, and the CH_4 7 times higher (values obtained by Reyes et al in [12]). For that reason, the Cordia Alliodora has a higher burning velocity than Pinus Patula.

In Fig. 11 also it is possible to see that Aramco kinetic mechanism gives similar values of the LBV for equivalence ratios >1.2.

The flame temperature of Pinus Patula and Cordia Alliadora BPGs is presented in Fig. 12i as a function of the equivalence ratio, and under 0.1 MPa and 363 K of initial conditions. There is a maximum for the flame temperature at the stoichiometric conditions due to the reaction rate, and higher values of gaseous fuels for Cordia Alliodora composition than the reached ones with the Pinus Patula BPG. The increment in initial temperature has a direct effect on flame temperature, and the variation of pressure has a nearly negligible influence. Adiabatic flame temperature results are in concordance with theoretical results, obtaining the highest value for stoichiometric conditions, and for mixtures with equivalence ratios lower or higher than the stoichiometric, flame temperature decreases. The difference in the compositions of Cordia Alliodora and Pinus Patula BPG are the reason why Cordia Alliodora has higher flame temperature values, as it was detailed before for the LBV of both mixtures. The influence of H_2 content can be explained given its high adiabatic flame temperature and thermal diffusivity [19].

CO, CO_2, NO_2 and NO emissions are presented in Fig. 13 for both BPG compositions. It is possible to see that the CO_2 emissions reach a maximum value near the stoichiometric mixture, for both BPG compositions, and Pinus Patula BPG combustion produces higher values of CO_2 emissions. CO emissions increase with the equivalence ratio for both BPG compositions, as it was expected.

The emissions of thermal NOx are formed by oxidation of nitrogen in air and require enough temperature and time to be produced, typically higher than 1800 K. The chemical reactions (highly temperature dependent) that control the thermal NOx are known as the extended Zeldovich mechanism [47]. Flame-generated NOx occurs in the flame front and there are several chemical mechanisms involved, which are associated to the intermediate species development in the flame front. In Fig. 13, the NOx mol fraction from BPG mixtures for different fuel/air equivalence ratios is also presented. The NO_2 values decrease with the equivalence ratio and remain nearly constant for rich mixtures (fuel/air equivalence ratios higher than 1.0). The behavior of NO_2 emissions is similar for both BPG, with the exception for 0.8 equivalence ratio where Cordia Alliodora has a higher value. NO emissions are presented in

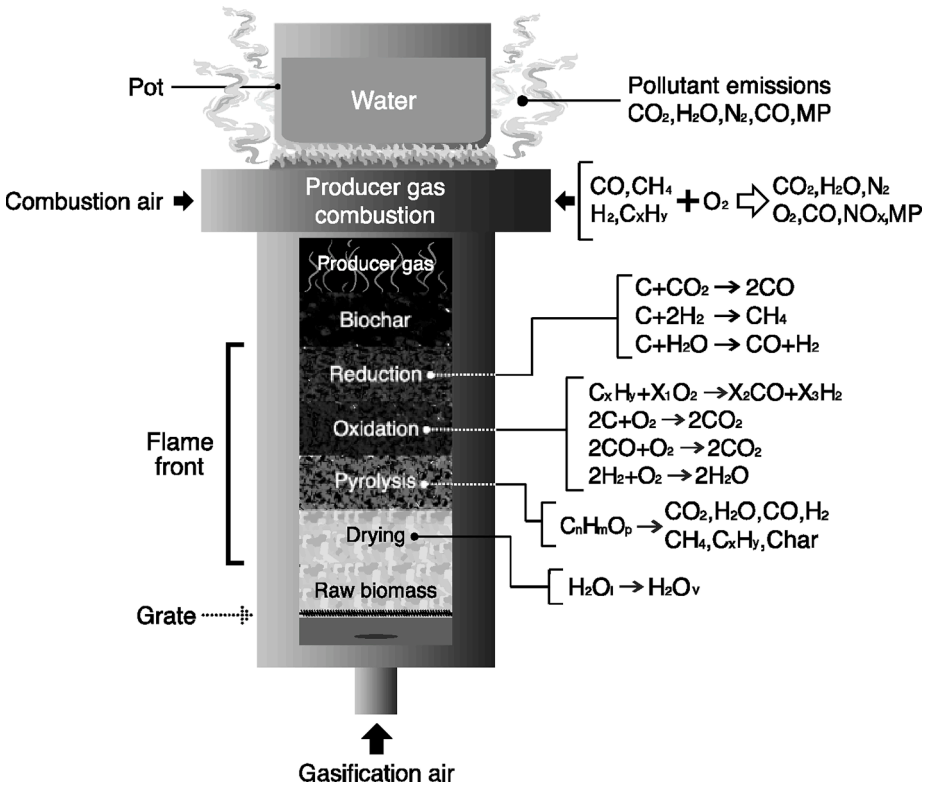

Fig. A1. Thermochemical process and producer gas combustion stage involved in a biomass gasification-based cookstove.

Fig. 14iv, where NO emissions for both BPG compositions (Pinus Patula and Cordia Alliodora) increase with the equivalence ratio until reaching its maximum value for an equivalence ratio of 1.1, at which point NO emissions begin to decrease. The NO emissions behavior is independent of BPG compositions due to the values of flame temperatures, which are lower than 1550 K. The thermal mechanism is the most important formation mechanism of NO at high temperatures, due to the oxidation of nitrogen present in atmospheric air. The formation of NO from N2 occurs through a mechanism chain reaction, initially proposed by Zeldovich [47]. The strong dependence on temperature makes the thermal mechanism no longer important at temperatures below 1800–2000 K, as it happens in this work. It is worth note the low value of NOx emissions obtained, where the mass fractions of NO are of the order of 10^{-6} and the order of NO_2 is of 10^{-9}, which is ascribed to the low value of the flame temperature (<1550 K).

Fig. 14 shows CO, CO_2 and NOx emissions versus the equivalence ratio to analyse the influence of the initial temperature in Pinus Patula BPG flames, where it is possible to see that the increment in initial temperature does not affect the CO nor CO_2 emissions. Fig. 14 also shows that NO emissions increase with the temperature, and NO_2 emissions are not visible affected, with the exception of 0.8 equivalence ratio.

Fig. 15 shows the emissions of Pinus Patula BPG as a function of fuel/air equivalence ratio for studying the effect of initial pressure. CO_2 emissions are slightly affected by the increment of the initial pressure under stoichiometric equivalence ratios, obtaining lower emissions for the lowest initial pressure. Concerning the NO emissions, the increment of initial pressure decreases NO emissions; an inverse effect is detected regarding the NO_2 emissions for low equivalence ratios. Nevertheless, the NO and NO_2 emissions are still low, especially NO_2 ones.

4. Conclusions

In this work a methodology to characterize the combustion process of biomass producer gas derived from a biomass gasification-based cookstove is presented. Two different biomass species have been investigated: Pinus Patula and Cordia Alliodora, which are forests species with dendro-energy potential in Colombia. Biomass producer gas compositions have been characterized in a constant volume combustion bomb instrumented for pressure register and image recording (Schlieren technique). Pressure evolution, burning velocity, flame radius, flame front speed, and flame morphology have been investigated for both BPG compositions, under different initial conditions of pressure, temperature, and equivalence ratio. The combustion study of the producer gas has been conducted out since the experimental and kinetic modelling point of views.

Though the Schlieren technique it can be seen that each one of the BPG compositions has a different flame front morphology: BPG coming from the Pinus Patula does not develop a cellular flame front at any conditions, meanwhile BPG coming from Cordia Alliodora develops a cellular flame front at high temperatures of 383 K.

Experimental results show that combustion processes with higher initial pressures (0.4 MPa) and lower initial temperatures (360 K) have the lower burning velocity (0.265 m/s), this value is one seventh of the CH4 burning velocity, and one fifteenth of the H2 burning velocity under the same conditions of pressure and temperature. In addition, kinetic modelling results show that burning velocity increases with the equivalence ratio until the value of 1.1, where decreases for mixtures with higher fuel/air equivalence ratios. Cordia Alliodora BPG presents higher burning velocities (around 11% higher) than Pinus Patula BPG, due to their difference in composition. BPG composition affects mainly the CO_2 emissions, so that higher CO_2 emissions are obtained during the combustion of Pinus Patula BPG. Values of NO and NO_2 emissions are very low, especially NO_2 emissions (of the order of 10^{-6} and 10^{-9}, respectively). Higher initial pressures (up to 0.4 MPa) and lower temperatures reduce NO emissions, while NO_2 increases with pressure (for fuel/air equivalence ratios lower than the stoichiometric). The BPG composition does not affect to the NO_x emissions.

Declaration of Competing Interest

The authors declare that they have no known competing financial interests or personal relationships that could have appeared to influence the work reported in this paper.

Data availability

Data will be made available on request.

Acknowledgements

The authors would like to thank the Spanish Ministry of Science and Innovation-Agencia Estatal de Investigación, for the financial support of this investigation with the research project PID2019-106957RB-C22. This work was developed under the support of the Research Group in Engines and Renewable Energies (MyER) from the University of Valladolid. The authors would like to thank to the University of Valladolid (Spain) for financial support for this research through the Visiting Professor Program for the Thermal Engines and Renewable Energies research group (MYER) from the Department of Energy and Fluid Mechanics Engineering.

Appendix 1. . Fundamental concepts of the biomass gasification-based cookstove

The biomass gasification-based cookstoves are also known as forced-draft or top-lit updraft cookstoves. The bed of our cookstove is a batch type reactor that is filled with solid biomass. Fig. A1 shows the thermochemical transformation processes into a gasification-based cookstove, as well as the BPG oxidation for producing hot gases (thermal energy) for cooking tasks. The solid fuel is ignited on the stove top, and the reaction front goes down losing heat through the wall until reach the grate [48,49]; thereby, the BPG heating value derived from a cookstove is lower than that of the downdraft gasifier-derived BPG [10]. The thermochemical reaction front is composed by the drying, pyrolysis and oxidation (pyro-combustion), and reduction stages [50]. The gasification air is supplied across the bottom section of the cookstove, which flows up through the biomass bed providing the necessary oxygen for transforming the wood biomass to a gaseous fuel. The heat released during the thermochemical process (oxygen lean biomass combustion stage) provide the required energy for the drying and pyrolysis stages of the fresh biomass, whilst the reaction front moves downwards until to reach the grate. This solid–gas transformation process is known as autothermal gasification [51]. The gases that leave from the lean oxidation stage flows through the biochar bed promoting the reduction stage where the concentrations of CO, H_2, and CH_4 increase [50]. The gasification global reaction of biomass in the fixed bed reactor is shown in Eq. A(1).

$$CH_xO_y + a(O_2 + 3.76N_2) + wH_2O \rightarrow n_1H_2 + n_2CO + n_3CO_2 + n_4H_2O + n_5CH_4 + n_6N2 + n_7C(char) + n_8C_nH_mO_p \quad (A1)$$

The BPG, mainly composed by CO, H_2, and CH_4, continue flowing upwards until the combustion chamber of the cookstove where the combustion-air is supplied (Fig. A1). The heat released by the homogeneous oxidation reaction is transferred to the pot. In the biomass cookstove considered here, the gasification and combustion air are supplied by means of forced-draft using small fans [49,52].

References

[1] Aberilla JM, Gallego-Schmid A, Stamford L, Azapagic A. Environmental sustainability of cooking fuels in remote communities: Life cycle and local impacts. Sci Total Environ 2020;713:136445.
[2] Jetter J, Zhao Y, Smith KR, Khan B, Yelverton T, DeCarlo P, et al. Pollutant emissions and energy efficiency under controlled conditions for household biomass cookstoves and implications for metrics useful in setting international test standards. Environ Sci Tech 2012;46(19):10827–34.
[3] Wilke J, Vogel O, Vogt L. Why are you running and does it hurt? Pain, motivations and beliefs about injury prevention among participants of a large-scale public running event. Int J Environ Res Public Health 2019;16(19):3766.
[4] Irena. World energy transitions outlook 2022: 1.5° C pathway. Int Renew Energy Agency Abu Dhabi 2022.
[5] Gitau JK, Sundberg C, Mendum R, Mutune J, Njenga M. Use of biochar-producing gasifier cookstove improves energy use efficiency and indoor air quality in rural households. Energies 2019;12(22):4285.
[6] Gupta A, Mulukutla AN, Gautam S, TaneKhan W, Waghmare SS, Labhasetwar NK. Development of a practical evaluation approach of a typical biomass cookstove. Environ Technol Innov 2020;17:100613.
[7] Chica E, Perez JF. Development and performance evaluation of an improved biomass cookstove for isolated communities from developing countries. Case Stud Therm Eng 2019;14:100435.
[8] Ismail O, Urbanus M, Murage H, Francis O. Conversion of rice husks into an energy source through gasification technology. Int J Sci Res (IJSR) 2016;5(9):1264–8.
[9] Tryner J, Tillotson JW, Baumgardner ME, Mohr JT, DeFoort MW, Marchese AJ. The effects of air flow rates, secondary air inlet geometry, fuel type, and operating mode on the performance of gasifier cookstoves. Environ Sci Tech 2016;50(17):9754–63.
[10] Gutiérrez J, Chica EL, Pérez JF. Parametric analysis of a gasification-based cookstove as a function of biomass density, gasification behavior, airflow ratio, and design. ACS Omega 2022;7(9):7481–98.
[11] Monteiro E, Rouboa A. Measurements of the laminar burning velocities for typical syngas–air mixtures at elevated pressures. J Energy Res Technol 2011;133(3).
[12] Reyes M, Tinaut FV, Horrillo A, Lafuente A. Experimental characterization of burning velocities of premixed methane-air and hydrogen-air mixtures in a constant volume combustion bomb at moderate pressure and temperature. Appl Therm Eng 2018;130:684–97.
[13] Reyes M, Sastre R, Tinaut F, Rodríguez-Fernández J. Study and characterization of the instabilities generated in expanding spherical flames of hydrogen/methane/air mixtures. Int J Hydrogen Energy 2022.
[14] Tinaut F, Reyes M, Melgar A, Giménez B. Optical characterization of hydrogen-air laminar combustion under cellularity conditions. Int J Hydrogen Energy 2019;44(25):12857–71.
[15] Reyes M, Sastre R, Giménez B, Sesma C. Experimental, kinetic modeling and morphologic study of the premixed combustion of hydrogen/methane mixtures. Energies 2022;15(10):3722.
[16] Wei Z, Zhen H, Fu J, Leung C, Cheung C, Huang Z. Experimental and numerical study on the laminar burning velocity of hydrogen enriched biogas mixture. Int J Hydrogen Energy 2019;44(39):22240–9.
[17] Williams FA. Combustion. In: Meyers RA, editor. Encyclopedia of physical science and technology. 3rd ed. New York: Academic Press; 2003. p. 315–38.
[18] Hernandez JJ, Lapuerta M, Serrano C, Melgar A. Estimation of the laminar flame speed of producer gas from biomass gasification. Energy Fuel 2005;19(5):2172–8.
[19] Andrade RV, Cortabarria Castañeda LA, Yepes Maya DM, Pedroso Cesar Corrêa Junior PS, Mello e Pinto LR, Silva Lora EE, et al. Assessment of laminar flame velocity of producer gas from biomass gasification using the Bunsen burner method. Int J Hydrogen Energy 2020;45(20):11559–68.
[20] Tinaut F, Melgar A, Giménez B, Reyes M. Characterization of the combustion of biomass producer gas in a constant volume combustion bomb. Fuel 2010;89(3):724–31.
[21] Martínez JD, Mahkamov K, Andrade RV, Silva Lora EE. Syngas production in downdraft biomass gasifiers and its application using internal combustion engines. Renew Energy 2012;38(1):1–9.
[22] Reyes M, Tinaut F, Giménez B, Camaño A. Combustion and flame front morphology characterization of H2–CO syngas blends in constant volume combustion bombs. Energy Fuel 2021;35(4):3497–511.
[23] Teh JS, Teoh YH, How HG, Idroas MY, Le TD, Nguyen HT. Experimental studies of combustion and emission characteristics of Biomass Producer Gas (BPG) in a Constant Volume Combustion Chamber (CVCC) System. Energies 2022;15(21):7847.
[24] Das AK, Kumar K, Sung C-J. Laminar flame speeds of moist syngas mixtures. Combust Flame 2011;158(2):345–53.
[25] Hernández JJ, Lapuerta M, Barba J. Flame stability and OH and CH radical emissions from mixtures of natural gas with biomass gasification gas. Appl Therm Eng 2013;55(1–2):133–9.

[26] Sukumaran S, Kong S-C. Modeling fuel NOx formation from combustion of biomass-derived producer gas in a large-scale burner. Combust Flame 2013;160(10):2159–68.
[27] Serrano C, Hernandez J, Mandilas C, Sheppard C, Woolley R. Laminar burning behaviour of biomass gasification-derived producer gas. Int J Hydrogen Energy 2008;33(2):851–62.
[28] Tryner J. Combustion phenomena in biomass gasifier cookstoves. Colorado State University; 2016.
[29] Kaundal A, Powar S, Dhar A. Solar-assisted gasification based cook stoves. coal and biomass gasification. Springer; 2018. p. 403–22.
[30] Hurtado Pérez E, Mulumba Ilunga O, Alfonso Solar D, Moros Gómez MC, Bastida-Molina P. Sustainable cooking based on a 3 kW air-forced multifuel gasification stove using alternative fuels obtained from agricultural wastes. Sustainability 2020;12(18):7723.
[31] Alliance CC. The water boiling test, version 4.2. 3: Cookstove emissions and efficiency in a controlled laboratory setting. Glob Alliances Clear Cookstoves 2013;2:52.
[32] Lenis YA, Agudelo AF, Pérez JF. Analysis of statistical repeatability of a fixed bed downdraft biomass gasification facility. Appl Therm Eng 2013;51(1–2):1006–16.
[33] Bilsback KR, Dahlke J, Fedak KM, Good N, Hecobian A, Herckes P, et al. A laboratory assessment of 120 air pollutant emissions from biomass and fossil fuel cookstoves. Environ Sci Tech 2019;53(12):7114–25.
[34] Goodwin DG, Moffat HK, Speth RL. Cantera: an object-oriented software toolkit for chemical kinetics, thermodynamics, and transport processes. version; 2018.
[35] Gregory P, Golden D, Frenklach M, Moriarty N, Eiteneer B, Goldenberg M, et al. GRI-Mech 3.0 (Tech. Rep.). UC Berkeley: Berkeley, CA, USA 2018.
[36] Hermanns R, Konnov A, Bastiaans R, De Goey L. Laminar burning velocities of diluted hydrogen− oxygen− nitrogen mixtures. Energy Fuel 2007;21(4):1977–81.
[37] Konnov AA. The temperature and pressure dependences of the laminar burning velocity: experiments and modelling. In: Proceedings of the European Combustion Meeting–2015. Budapest, Hungary; 2015.
[38] Goswami M, Derks SCR, Coumans K, Slikker WJ, de Andrade Oliveira MH, Bastiaans RJM, et al. The effect of elevated pressures on the laminar burning velocity of methane+air mixtures. Combust Flame 2013;160(9):1627–35.
[39] Clarke A. Measurement of laminar burning velocity of air/fuel/diluent mixtures in zero gravity. University of Oxford; 1994.
[40] Metghalchi M, Keck JC. Laminar burning velocity of propane-air mixtures at high temperature and pressure. Combust Flame 1980;38:143–54.
[41] Wang T, Zhang X, Zhang J, Hou X. Automatic generation of a kinetic skeletal mechanism for methane-hydrogen blends with nitrogen chemistry. Int J Hydrogen Energy 2018;43(6):3330–41.
[42] Zhou Q, Cheung C, Leung C, Li X, Li X, Huang Z. Effects of fuel composition and initial pressure on laminar flame speed of H2/CO/CH4 bio-syngas. Fuel 2019;238:149–58.
[43] Lafuente A. Metodología para el diagnóstico de la velocidad de combustión laminar de mezclas de gases combustibles a partir de la medida de la presión instantánea en una bomba de combustión a volumen constante. University of Valladolid; 2008.
[44] Serrano C. Estudio del comportamiento del gas de gasificación de biomasa en procesos de combustión. Universidad de Castilla la Mancha; 2006.
[45] Vagelopoulos C, Egolfopoulos F. Laminar flame speeds and extinction strain rates of mixtures of carbon monoxide with hydrogen, methane, and air. *Symposium (international) on combustion.* 25. Elsevier; 1994:1317-23.
[46] Scholte T, Vaags P. The influence of small quantities of hydrogen and hydrogen compounds on the burning velocity of carbon monoxide-air flames. Combust Flame 1959;3:503–10.
[47] Lavoie GA, Heywood JB, Keck JC. Experimental and theoretical study of nitric oxide formation in internal combustion engines. Combust Sci Technol 1970;1(4):313–26.
[48] Birzer C, Medwell P, Wilkey J, West T, Higgins M, MacFarlane G, et al. An analysis of combustion from a top-lit up-draft (TLUD) cookstove. J Human Eng 2013;2(1).
[49] Mehta Y, Richards C. Gasification performance of a top-lit updraft cook stove. Energies 2017;10(10):1529.
[50] Pérez JF, Benjumea PN, Melgar A. Sensitivity analysis of a biomass gasification model in fixed bed downdraft reactors: effect of model and process parameters on reaction front. Biomass Bioenergy 2015;83:403–21.
[51] Sutar KB, Kohli S, Ravi M, Ray A. Biomass cookstoves: a review of technical aspects. Renew Sustain Energy Rev 2015;41:1128–66.
[52] Obi OF, Ezeoha SL, Okorie IC. Energetic performance of a top-lit updraft (TLUD) cookstove. Renew Energy 2016;99:730–7.